Heat disproportionately kills young people:

evidence from wet-bulb temperature in Mexico

Andrew J. Wilson[‡1,2,3,4], R. Daniel Bressler[‡*1,2,3], Catherine Ivanovich[2,5], Cascade Tuholske[6], Colin Raymond[7,8], Radley M. Horton[2,5], Adam Sobel[2,6,9], Patrick Kinney[10], Tereza Cavazos[11], and Jeffrey G. Shrader[1,2,3]

[1]School of International and Public Affairs, Columbia University
[2]Climate School, Columbia University
[3]Center For Environmental Economics and Policy, Columbia University
[4]Global Policy Laboratory, UC Berkeley
[5]Department of Earth and Environmental Sciences, Columbia University
[6]Department of Earth Sciences, Montana State University
[7]Joint Institute for Regional Earth System Science and Engineering, University of California, Los Angeles
[8]NASA Jet Propulsion Laboratory
[9]Department of Applied Physics and Applied Mathematics, Columbia University
[10]School of Public Health, Boston University
[11]Department of Physical Oceanography, CICESE, B.C., Mexico
[‡]Equal contribution
[*]Correspondence: rdb2148@columbia.edu

August 1, 2024

Abstract

Recent studies project that temperature-related mortality will be the largest source of future damage from climate change, with particular concern for the elderly (whom it is believed bear the largest heat-related mortality risk) and humid heat extremes (which physiology suggests may have dire consequences for human health). Here, we study heat and mortality in Mexico, a country that exhibits a unique combination of universal mortality microdata and among the most extreme humid heat exposures. By combining detailed measurements of wet-bulb temperature with granular, age-specific outcome data, we find that younger people are particularly vulnerable to heat while older people are particularly vulnerable to cold: those under 35 years old account for 75% of recent heat-related deaths and 87% of heat-related lost life years while those 35 and older account for 98% of cold-related deaths and 90% of cold-related lost life years. We develop high-resolution projections of humid heat and associated outcomes holding historically observed exposure–response relationships constant. We find that climate change causes temperature-related mortality risk in Mexico to shift from older people (more vulnerable to cold) to younger people (more vulnerable to heat). In the end of the 21^{st} century in the

SSP 3-7.0 emissions scenario, we project a 32% increase in temperature-related deaths among under-35-year-olds and a 33% decrease among those 35 and older.

1 Introduction

Historically, temperature exposure has caused a large number of premature deaths [1–3]. Heat-related mortality is expected to increase under climate change [4–27]. As the evidence base has grown, multiple studies have found that the elderly are especially vulnerable to heat [6, 11, 14, 17, 18, 28, 29]. Furthermore, many other studies have expressed particular concern for joint heat and humidity extremes, given the importance of perspiration for human thermoregulation [30–36].

In this study, we explore the relationship between humid heat and mortality in Mexico, a country that exhibits a unique combination of rich age-specific universal mortality microdata and among the most extreme historical humid heat exposures. We find that historically, the majority of heat-related mortality in Mexico has been concentrated among younger people: 75% of heat-related deaths and 87% of heat-related lost life years occur among those under 35 years old. Whereas the vast majority of cold-related mortality is concentrated among older people: 98% of cold-related deaths and 90% of cold-related lost life years occur among those over 35. We then develop projections of humid heat and associated outcomes to assess the future implications of these findings. As in other studies, we find that climate change is expected to increase heat-related mortality while decreasing cold-related mortality in our setting. However, we uncover an important source of future climate-driven inequality: the disproportionate impact of heat and cold across age groups reallocates the temperature-related mortality burden from the elderly (who are more impacted by cold) to the young (who are more impacted by heat). This has important implications for understanding the distributional impacts of climate change and for preparing effective policies to adapt to these impacts.

2 Analysis

Our insights into the effect of humid heat across the lifespan result from a combination of four elements: (1) station-level wet-bulb temperature estimates; (2) high-quality, age-specific, population-wide mortality microdata; (3) a statistical method that resolves age-specific heterogeneity in temperature vulnerability; and (4) realistic, granular projections of humid heat under climate change

across our study area.

First, we study the effect of *wet-bulb temperature* on mortality. While multiple metrics exist to measure humid heat stress [37], wet-bulb temperature has been identified as an important metric for understanding the impact of heat on human health because it accounts for the critical role of sweat evaporation—the primary mechanism by which the human body cools itself—in maintaining homeostasis under heat exposure [36, 38]. Under high humidity, sweating efficiency decreases [37, 39, 40]. When ambient wet-bulb temperature exceeds human skin temperature (at around 35°C), humans can no longer dissipate heat into the environment and are thus physically incapable of survival when exposed for a sufficient length of time [30, 32, 33]. In practice, experimental evidence has shown that heat stress can become uncompensable at wet-bulb temperatures of 31°C or lower depending on meteorological conditions and individuals' physiology [34, 35]. Under high emissions scenarios, increasing humid heat stress is projected to cause some regions to become uninhabitable for parts of the year without artificial cooling [33]. Despite the importance of both heat and humidity for human thermoregulation, most empirical studies on temperature-related mortality have focused on dry-bulb temperature, which does not account for humidity.[1]

Second, our study leverages precise historical data on both mortality and temperature exposure. Mexico's high-quality vital statistics microdata includes a record of each death occurring in the country since 1998. Crucially, these microdata also contain information on age at death, allowing us to assess age-specific heterogeneity in the relationship of heat and mortality with more precision than prior literature, which has focused on broader age groups or on effects only among the elderly [6, 12, 36, 41]. Over the 22 years from 1998 to 2019,[2] the data contain information on the day and municipality[3] of occurrence of 13.4 million deaths over more than 21 million municipality–days. We combine these records with station-level measurements of temperature, humidity, and pressure, which we use to develop estimates of local daily mean wet-bulb temperature [42]. This is important because we find evidence that weather reanalysis data products such as ERA5-Land

[1] Hundreds of papers have been written on the mortality impact associated with dry-bulb temperature [4, 8]. One review found only nine papers that assessed the role of humid heat on mortality [31], and there remain important gaps in our understanding of the population-wide health impacts of humid heat [36].

[2] We choose to end our study period in 2019, before the COVID-19 pandemic.

[3] Mexico's second-order administrative unit, numbering around 2400 across the country

do not reproduce the most extreme humid heat events observed by Mexico's station network (see Figure S13). Mexico's heterogeneous climate and rich public vital statistics records make it an ideal setting for determining the impact of humid heat exposure on premature mortality. Mexico is one of the most climatically diverse countries in the world, with the fourth largest number of Köppen climate zones (see Figure S14). It is located in the subtropics and tropical regions, has a wide variety of elevations, is located between two oceans, and experiences substantial seasonal variation, including the North American monsoon. The low correlation between air temperature and humidity observed throughout many areas of Mexico [36] allows extreme dry and humid heat events to take place on separate days within the same location, facilitating the investigation of the distinct impacts of these two extreme types. Most existing studies have assessed temperature-mortality relationships in cooler, higher-income countries [30, 36] that have never experienced humid heat extremes. Mexico, by contrast, has experienced among the highest wet-bulb temperatures ever recorded [32]. Substantial populations are also exposed to these diverse climates across the country (see Figure S14).

Third, we estimate an age-specific exposure relationship between excess mortality and daily average wet and dry-bulb temperature. Our empirical model leverages current best practices to isolate causal impacts of temperature on excess mortality [1, 6]. We investigate effects over a set of distributed lags to capture the dynamic effects of temperature on health, including harvesting (when "deaths are occurring only a few days early among persons who were already dying" [43])and delayed mortality responses. Our model flexibly captures differences in impacts from cold, moderate, and hot temperature exposures and includes control variables to account for potential confounders, including seasonality and time trends. We identify effects based on otherwise random changes in weather across days within a given municipality, such that a municipality experiencing mild weather acts as the "control group" for itself during more extreme weather, eliminating confounding spatial variation. Lastly, we flexibly adjust for daily precipitation to ensure that the effects of temperature are not operating via rainfall. Importantly, our statistical model allows the minimum mortality temperature (MMT) to vary by age group. We find that different age groups experience minimum mortality at substantially different temperatures: individuals in their 70s experience minimum

mortality at temperatures nearly 10°C higher than individuals in their 20s for both dry-bulb and wet-bulb temperatures (see Figure S11 below). See Section A.2 for further details on the model and estimation procedure.

Finally, we develop fine-scale projections of dry and humid heat through the end of the century to project changes in mortality across age groups as the climate warms. We retrieve statistically down-scaled temperature, humidity, and precipitation projections through the end of the century [44] across four greenhouse gas emission (SSP-RCP) scenarios [45]; calculate wet-bulb temperature; and bias correct the dry-bulb temperature, wet-bulb temperature, and precipitation projections against historical station and reanalysis data [46, 47] using percentile mapping. This approach allows us to best match the spatial distribution of the available human health data, as well as to capture the variability in climate and terrain throughout Mexico, essential to reproducing dry and humid heat extremes [48]. For additional details, see Section A.1.2.

3 Results

Figure 1 shows the effect of exposure to a single day at the indicated wet-bulb temperature on mortality risk for different age groups. For instance, the under-5 exposure–response function implies that when an individual under 5 years of age experiences one day with average wet-bulb temperature of 27°C, their risk of mortality increases by 45% relative to if they had experienced one day with an average wet-bulb temperature of 13°C. (For policymakers, numerical values for the estimated additional number of deaths per person for different temperature exposures are shown in Table S1.) Figure 2 (left panel) combines the age-specific vulnerability to heat and cold (shown in Figure 1 top panel) along with the frequency with which those temperatures occur (shown in Figure 1 bottom panel) to quantify the total annual number of temperature-related deaths associated with exposure to temperature broken down into one-degree temperature bins and broken out by age-group during our historical data period. In Figure 3, points labeled "Historical" aggregate this data to quantify the total annual number of heat and cold-related deaths by age group. These values combine age-specific vulnerability to heat and cold (shown in the top panels of Figure 1) with the frequency

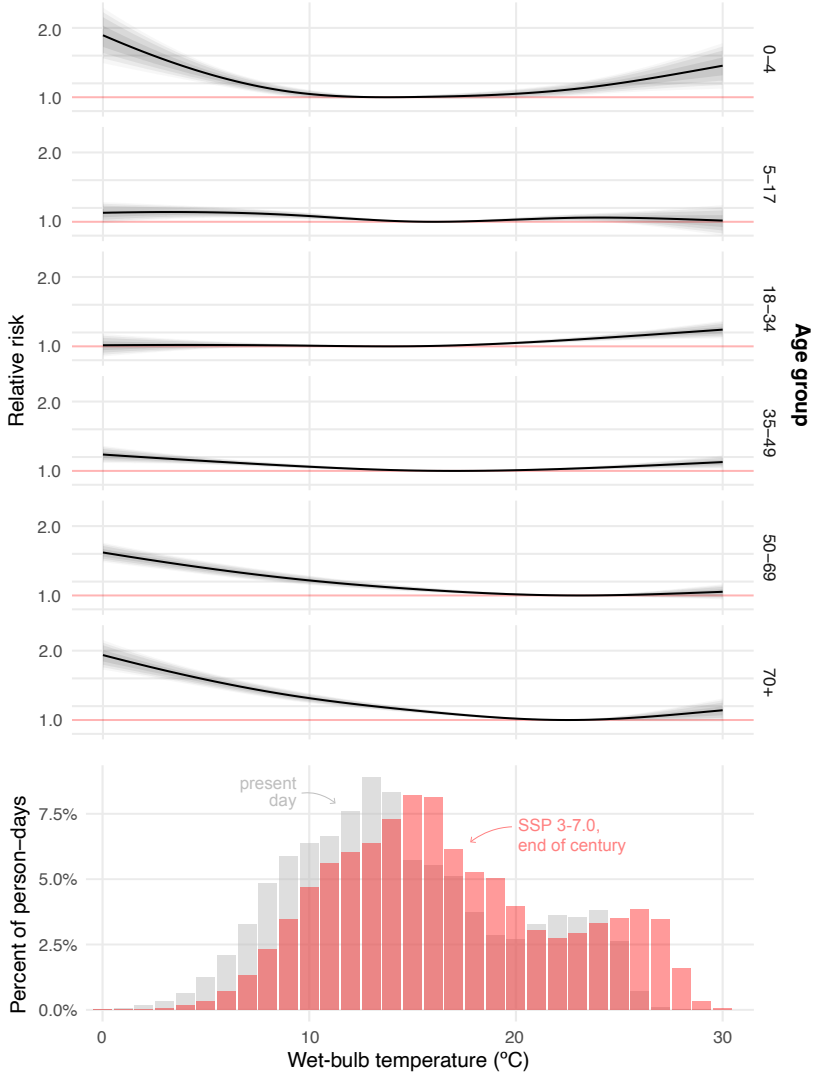


Figure 1: Relationships between mortality risk and exposure to wet-bulb temperature by age group in Mexico

The top panels show the change in relative mortality risk (y-axis) caused by exposure to one day of the indicated average daily wet-bulb temperatures (x-axis) across age groups. The bottom panel shows the distribution of daily average wet-bulb temperatures in Mexico throughout our sample period as well as the ensemble mean of projected temperature distribution at the end of the century (2083–2099) under the SSP 3-7.0 emission scenario. Shaded bands around the functions in the top panels indicate 95, 90, 80, and 50% confidence intervals. Absolute changes in mortality for both wet- and dry-bulb temperature are shown in Figure S1, and coefficient estimates for absolute mortality changes are shown in Table S1.

with which those temperatures occur (shown in the bottom row of Figure 1).

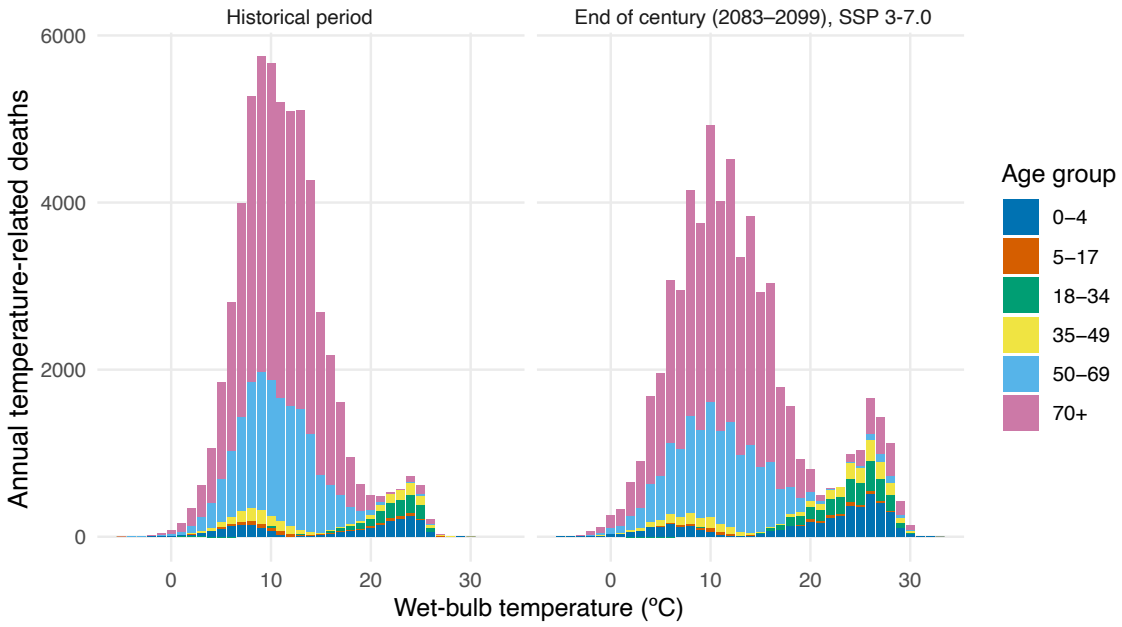


Figure 2: Historical and projected annual temperature-related deaths in Mexico
The panels show average annual temperature-related deaths resulting from exposure to days with the average wet-bulb temperatures shown on the x-axis during the historical period (left panel) and at the end of the century (2083–2099) under the SSP 3-7.0 emission scenario (right panel) across six age groups in Mexico. The figure shows mean projected deaths; see Figure 3 for projections with uncertainty.

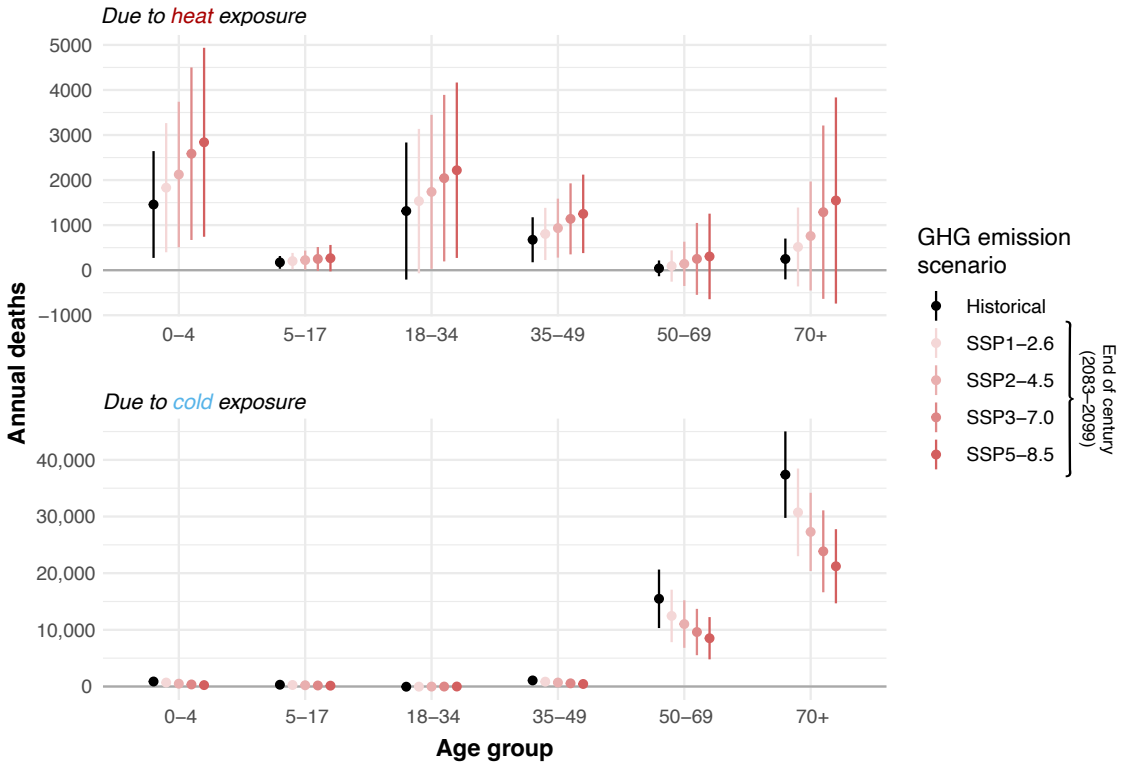


Figure 3: Historical and projected annual deaths due to heat (top panel) and cold exposure (bottom panel) by age group
The figure depicts the average annual number of deaths attributed to heat and cold exposure in Mexico historically and under wet-bulb temperatures prevailing at the end of the century in four greenhouse gas emission scenarios. Whiskers above and below each estimate depict 95% confidence intervals net of both econometric and climate uncertainty. Note that the range of the y-axis in the bottom panels is roughly eight times the range of the y-axis in the top panels.

Consistent with past literature on temperature-related mortality in Mexico [28, 49], we find that cold is historically associated with more deaths than heat across the whole population: cold causes 14 times more deaths than heat, as shown in Figure 3. However, this masks important heterogeneity across age groups. While cold-related mortality is concentrated among the old, heat-related mortality is concentrated among the young. For individuals under 35, heat causes 2.6 times *more* deaths than cold (Figure 3, top panel). Whereas for individuals 35 and older, cold causes 56 times more deaths than heat (Figure 3, bottom panel). 98% of cold-related deaths occurred

among those 35 and older, whereas 75% of heat-related deaths occurred among under-35-year-olds (the distributions of these proportions are shown in Figure S5). This contrasts with the previous literature, which has found that both cold and heat-related mortality impacts are concentrated among elderly people.

When considering lost life years, which accounts for the fact that younger individuals have on average more remaining life than older individuals, the outsized impact of heat on younger age groups becomes even more pronounced (Figure 4): those under 35 years old account for 87% of life years lost due to recent heat exposure, whereas those 35 and older account for 90% of life years lost to recent cold exposure.

We find that these results around the concentration of the heat-related mortality burden among the young and the cold-related mortality burden among the old are robust whether we use wet- or dry-bulb temperature as our metric of exposure (as shown in Figures S1, S2, S3, S4, and S5). Although, importantly, nearly all historical exposures—even in our context—are below uncompensable humid heat levels [34, 50].

The right panel of Figure 2 and the red points and whiskers in Figure 3 show our projections for the number of annual deaths at the end of the century broken down by age group. These projected deaths do not account for potential future adaptation or population changes, but rather describe the effect of projected future temperatures on mortality given historical socioeconomic, institutional, and adaptation conditions. Climate change is projected to cause more heat-related mortality and less cold-related mortality across all age groups. Cold-related mortality continues to be concentrated among individuals 35 and older, while heat-related mortality continues to be concentrated among individuals under 35 years old. However, as hot days become more frequent and cold days become less frequent, the overall temperature-related mortality burden shifts towards the young and away from the old. Those 35 and older continue to suffer disproportionately from cold-related mortality, but cold days are comparatively less frequent. Those under 35 suffer disproportionately from increasing heat, with premature mortality especially concentrated in the under-5 and 18–34 age groups.

Figures 3 and S6 show the projected percent change in age group temperature-related deaths at

the end of the century across four different greenhouse gas emission scenarios, ranging from a rapid decarbonization scenario (SSP 1-2.6) to a very high emissions scenario (SSP 5-8.5). All results are relative to historical temperature-related deaths. These figures show that the age structure of mortality burdens in Figure 2 holds more generally across low, medium, and high emissions scenarios. In all scenarios, climate change shifts the risk of temperature-related mortality toward those under 35 and away from those 35 and older. Under the SSP 3-7.0 emission scenario, we project a 32% increase in temperature-related deaths among under-35-year-olds driven by an increase in heat-related mortality, and a 33% decrease among those 35 and older driven by a decrease in cold-related mortality (the distribution of these estimates of percent changes in overall temperature-related mortality are shown in Figures S6 and S7).

Previous research has shown that dry-bulb temperature-related mortality in Mexico is currently driven primarily by cold [49] and that under climate change, temperature-related mortality will fall in Mexico as the benefits from reduced cold outweigh the harms from increased heat [6]. Our results present a more complicated picture: we find—consistent with prior literature—that temperature-related mortality as a whole will fall in Mexico under climate change, but when taking age-specific effects into account, we project that this will happen at the expense of younger individuals.

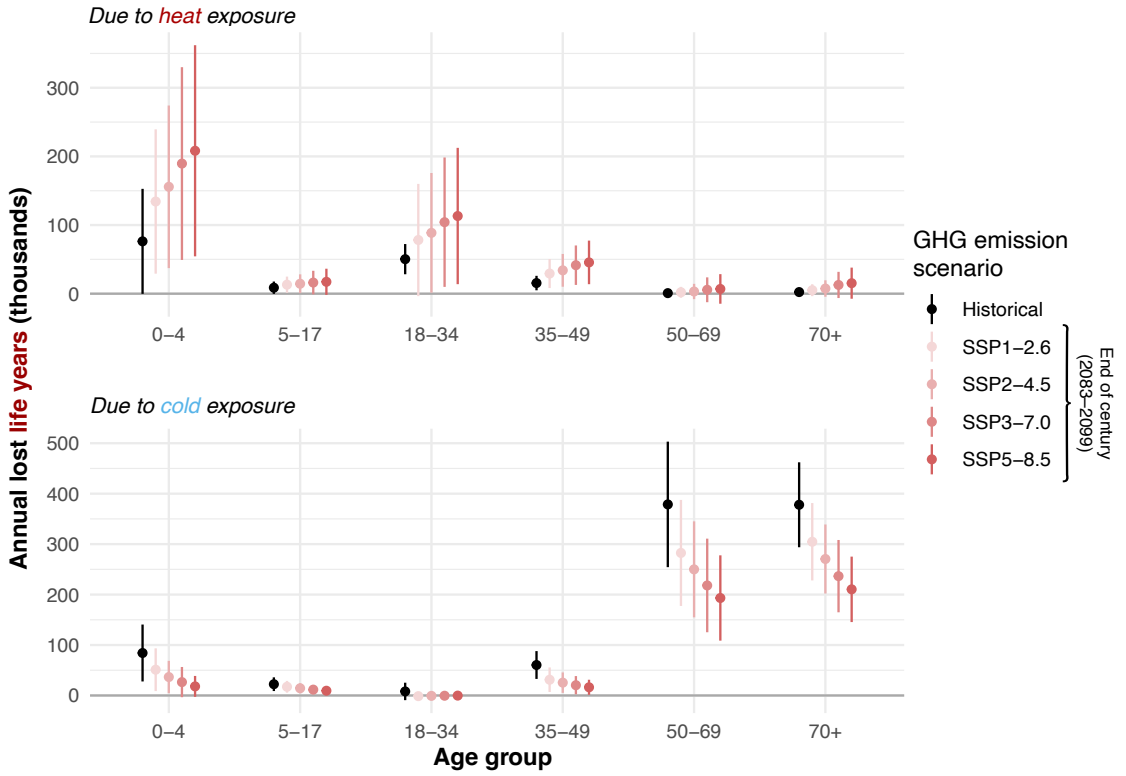


Figure 4: Historical and projected annual lost life years due to heat (top panel) and cold (bottom panel) exposure by age group
This figure mirrors Figure 3, but with the outcome as lost life years, rather than deaths. Potential remaining life years are taken from the UN World Population Prospects 2022, and are aggregated to time-invariant age group values by taking a population-weighted average across single age bins and years. The figure depicts the annual number of lost life years attributed to heat and cold exposure in Mexico historically and under wet-bulb temperatures prevailing at the end of the century in four greenhouse gas emission scenarios. The top panel indicates values for heat exposure, whereas the bottom panel indicates values for cold exposure. Whiskers above and below each estimate depict 95% confidence intervals net of both econometric and climate uncertainty.

4 Discussion

The unique combination of elements in this study—station-level wet-bulb temperature estimates, granular mortality data from across the entire age distribution in a country with a wide diversity of climatic conditions, a statistical method that captures age-specific heterogeneity in temperature

vulnerability, and precise measurements of humid heat—reveals multiple novel aspects of the impact of temperature on mortality. By focusing on granular age-specific temperature-mortality impacts, our study contributes to the existing literature that has usually focused on mortality irrespective of age [1, 8, 51], across broader age groups [6], or on the elderly [12, 13]. In particular, in our setting, we find that while individuals 35 and older suffer the vast majority of the cold-related mortality burden, those younger than 35 people suffer the majority of the heat-related mortality burden. In addition, we identify a novel source of climate-driven inequality: across all future emissions scenarios, we find that climate change causes the temperature-related mortality burden to shift away from the elderly towards the young. Given that temperature-related mortality is projected to be the largest single source of climate damages [52, 53], the disproportionate burden of this impact on the young is likely an important source of future climate-driven inequality.

Older individuals are believed to be vulnerable to extreme temperatures for physiological, behavioral, and social reasons. First, the elderly are particularly susceptible to both hypothermia and hyperthermia because they exhibit lower shivering temperature thresholds [54], significantly lower levels of brown adipose tissue (key for non-shivering thermogenesis) [55], and have a lower whole-body sweat rate [56]. Second, a relatively large proportion of elderly individuals have pre-existing medical conditions that make them more vulnerable to the effects of extreme temperature or attendant respiratory illnesses [57]. Third, many medications used by the elderly can affect the body's ability to regulate temperature [41, 58]. Fourth, elderly individuals are increasingly living alone, making it more difficult for them to access public health resources during extreme weather events, and they experience higher rates of loneliness which is correlated with worse cardiovascular health [59, 60]. Fifth, energy poverty—spending a large fraction of income on energy—can be particularly acute for elderly individuals. Mexico has both a high rate of energy poverty and a high prevalence of credit constraints that might prevent adoption of protective but energy-intensive durable household goods like air conditioners [61, 62]. In this study, we indeed find that the elderly are quite vulnerable to both heat and cold (as shown in Figure 1) and that the elderly are, in terms of absolute mortality impacts, far more vulnerable to cold than other age groups (Figure S1). We find that the vast majority of cold-related mortality is concentrated in those 50 and older, as shown

in the top panels of Figure 2. However, we find that young people are particularly vulnerable to heat: the majority of heat-related deaths are concentrated in those under 35, and those under 35 are overrepresented in heat-related deaths relative to their fraction of the population despite their far lower background crude death rate (Figure S5).

Our finding that children younger than five years old are especially vulnerable to heat (Figure 1) is not inconsistent with prior work, although we find particularly acute effects. Multiple potential mechanisms may contribute to this result. First, infants have a higher body surface area to body weight ratio than adults, which means the gain heat more rapidly and are more susceptible to overheating; infants also have a less developed thermoregulatory system (exhibiting reduced sweating), which means they are not as efficient at regulating their body temperature [63]. Second, very young children have less well-developed immune systems, making them more vulnerable to climate-related infectious diseases including vector-borne diseases and diarrheal diseases that might be especially affected by humid heat [64, 65]. Finally, both infants and young children have less freedom of movement than adults and may not be able to express their discomfort or distress as easily as adults, making it more difficult for caregivers—the primary providers of child adaptation to heat exposure—to recognize and respond to their heat stress [66]. We also find that those 18 to 34 years old are very vulnerable to heat. This may be due to behavioral, social, and economic factors: although younger adults may be more physiologically robust to heat, they also likely experience more exposure to extreme heat in outdoor occupations with minimal flexibility for precautionary action [28, 67].

Our finding that young people in Mexico are especially vulnerable to heat may have global implications because hotter and lower-income countries—which are expected to be the most adversely impacted by climate change—have among the youngest populations in the world currently and over the coming century [68]. Figure S12 shows the current global pattern of age and wet-bulb temperature exposure. The map in the top panel breaks down countries by their most extreme wet-bulb temperatures and fraction of population younger than 35 years of age [69]. The youngest and hottest locations in the world are concentrated in Africa, Central America, the Middle East, and portions of Asia including Pakistan—the site of multiple, recent extreme heat waves.

The bottom panel of Figure S12 situates Mexico in the context of the rest of the world. Mexico is near the middle of the global distribution of countries by share of population under 35, and its extreme wet-bulb temperatures are essentially only surpassed by countries in Asia. The figure also shows that historical exposure to hot wet-bulb temperature is positively correlated with the fraction of the population under 35. If our age-specific results in this study hold for other countries around the world that are younger and hotter, then existing estimates of temperature-related mortality impacts in these countries—which neither fully capture age-specific heterogeneity in the temperature–mortality relationship nor account for the impact of humid heat—may be incorrect. In past work, the lack of age-specific mortality data has been a limiting factor in exploring the age-specific temperature-mortality relationship across a large number of countries [6, 51], which underscores the need for improvements in vital statistics systems, especially in the nations most vulnerable to climate change.

We conclude by highlighting a few important caveats and also point to potential areas of focus for future work. Recent work has pioneered the use of both temperature and humidity for constrained joint projections [38, 70, 71]. While regional and global climate models are our best tools for assessments of future heat stress risk, the relatively coarse time resolution of most model output limits the ability to project extreme values. The NEX-GDDP dataset used in this study reports variables at a daily resolution, like many other climate models. Given the misalignment of the diurnal cycles of temperature and humidity, using available daily mean values to calculate heat stress metrics such as wet-bulb temperature limits the accuracy of daily mean projections, and is virtually impossible for daily maximum projections. These data challenges relating to the sub-daily fluctuations in individual variables are even more pronounced for heat stress metrics such as wet-bulb globe temperature (WBGT) that incorporate additional variables relevant to the physiology of heat stress (e.g., solar insolation and wind speed) [72]. These limitations underpin efforts to increase the temporal resolution of model data output available to end users in order to better represent the most extreme heat stress conditions of the future.

Finally, our projections assume that our estimated temperature–mortality relationships will remain unchanged under future warming. There are opposing reasons why the exposure–response

functions to wet-bulb temperature may become either more or less severe in the future. Research on the U.S. shows that mortality vulnerability to non-optimal dry-bulb temperatures has decreased historically [73, 74], and a similar pattern could hold in Mexico. However, as wet-bulb temperatures approach uncompensable levels with significantly greater frequency [34, 50]—exposures of this degree are almost nonexistent in the historical record—we may learn that mortality associated with a given level of humid heat exposure is worse than existing estimates. Furthermore, the greater frequency of extremely hot days in future projections could reduce the ability of workers in outdoor industries to reallocate their labor away from working during adverse conditions. We leave the exploration of these questions to future work.

References

1. Gasparrini, A. *et al.* Mortality risk attributable to high and low ambient temperature: a multicountry observational study. en. *The Lancet* **386,** 369–375. ISSN: 01406736. https://linkinghub.elsevier.com/retrieve/pii/S0140673614621140 (2021) (July 2015).

2. Mitchell, D. *et al.* Attributing human mortality during extreme heat waves to anthropogenic climate change. en. *Environmental Research Letters* **11.** Publisher: IOP Publishing, 074006. ISSN: 1748-9326. https://doi.org/10.1088%2F1748-9326%2F11%2F7%2F074006 (2020) (July 2016).

3. Vicedo-Cabrera, A. M. *et al.* The burden of heat-related mortality attributable to recent human-induced climate change. en. *Nature Climate Change* **11,** 492–500. ISSN: 1758-678X, 1758-6798. http://www.nature.com/articles/s41558-021-01058-x (2021) (June 2021).

4. Bressler, R. D. The mortality cost of carbon. en. *Nature Communications* **12,** 4467. ISSN: 2041-1723. https://www.nature.com/articles/s41467-021-24487-w (2021) (July 2021).

5. Bressler, R. D., Moore, F. C., Rennert, K. & Anthoff, D. Estimates of country level temperature-related mortality damage functions. en. *Scientific Reports* **11,** 20282. ISSN: 2045-2322. https://www.nature.com/articles/s41598-021-99156-5 (2021) (Dec. 2021).

6. Carleton, T. *et al.* Valuing the global mortality consequences of climate change accounting for adaptation costs and benefits. en. *The Quarterly Journal of Economics,* 69 (2022).

7. Chen, K. *et al.* Impact of climate change on heat-related mortality in Jiangsu Province, China. en. *Environmental Pollution* **224,** 317–325. ISSN: 0269-7491. http://www.sciencedirect.com/science/article/pii/S0269749116319303 (2020) (May 2017).

8. Cromar, K. R. *et al.* Global Health Impacts for Economic Models of Climate Change: A Systematic Review and Meta-Analysis. eng. *Annals of the American Thoracic Society* **19,** 1203–1212. ISSN: 2325-6621 (July 2022).

9. Deschênes, O. & Greenstone, M. Climate Change, Mortality, and Adaptation: Evidence from Annual Fluctuations in Weather in the US. *American Economic Journal: Applied Economics* **3,** 152–185. ISSN: 1945-7782. https://www.jstor.org/stable/41288654 (2018) (2011).

10. Gasparrini, A. *et al.* Projections of temperature-related excess mortality under climate change scenarios. en. *The Lancet Planetary Health* **1,** e360–e367. ISSN: 25425196. https://linkinghub.elsevier.com/retrieve/pii/S2542519617301560 (2019) (Dec. 2017).

11. Hajat, S., Vardoulakis, S., Heaviside, C. & Eggen, B. Climate change effects on human health: projections of temperature-related mortality for the UK during the 2020s, 2050s and 2080s. en. *J Epidemiol Community Health* **68,** 641–648. ISSN: 0143-005X, 1470-2738. https://jech.bmj.com/content/68/7/641 (2020) (July 2014).

12. Hales, S. *et al. Quantitative risk assessment of the effects of climate change on selected causes of death, 2030s and 2050s* en. OCLC: 897764432. ISBN: 978-92-4-150769-1. http://apps.who.int/iris/bitstream/10665/134014/1/9789241507691_eng.pdf (2019) (2014).

13. Honda, Y. *et al.* Heat-related mortality risk model for climate change impact projection. en. *Environmental Health and Preventive Medicine* **19,** 56–63. ISSN: 1347-4715. https://environhealthprevmed.biomedcentral.com/articles/10.1007/s12199-013-0354-6 (2019) (Jan. 2014).

14. Houser, T. *et al. Economic Risks of Climate Change: An American Prospectus* en. Google-Books-ID: 0QTSBgAAQBAJ. ISBN: 978-0-231-53955-5 (Columbia University Press, Aug. 2015).

15. Kingsley Samantha L., Eliot Melissa N., Gold Julia, Vanderslice Robert R. & Wellenius Gregory A. Current and Projected Heat-Related Morbidity and Mortality in Rhode Island. *Environmental Health Perspectives* **124,** 460–467. https://ehp.niehs.nih.gov/doi/full/10.1289/ehp.1408826 (2020) (2016).

16. Knowlton, K. *et al.* Projecting Heat-Related Mortality Impacts Under a Changing Climate in the New York City Region. en. *American Journal of Public Health* **97,** 2028–2034. ISSN: 0090-0036, 1541-0048. http://ajph.aphapublications.org/doi/10.2105/AJPH.2006.102947 (2020) (Nov. 2007).

17. Kim, D.-W., Deo, R. C., Chung, J.-H. & Lee, J.-S. Projection of heat wave mortality related to climate change in Korea. en. *Natural Hazards* **80,** 623–637. ISSN: 0921-030X, 1573-0840. http://link.springer.com/10.1007/s11069-015-1987-0 (2020) (Jan. 2016).

18. Lee, J. Y. & Kim, H. Projection of future temperature-related mortality due to climate and demographic changes. en. *Environment International* **94,** 489–494. ISSN: 0160-4120. http://www.sciencedirect.com/science/article/pii/S0160412016302252 (2020) (Sept. 2016).

19. Li, T., Horton, R. M. & Kinney, P. L. Projections of seasonal patterns in temperature- related deaths for Manhattan, New York. en. *Nature Climate Change* **3,** 717–721. ISSN: 1758-6798. https://www.nature.com/articles/nclimate1902 (2020) (Aug. 2013).

20. Marsha, A., Sain, S. R., Heaton, M. J., Monaghan, A. J. & Wilhelmi, O. Influences of climatic and population changes on heat-related mortality in Houston, Texas, USA. en. *Climatic Change* **146,** 471–485. ISSN: 0165-0009, 1573-1480. http://link.springer.com/10.1007/s10584-016-1775-1 (2020) (Feb. 2018).

21. Martínez-Solanas, È. *et al.* Projections of temperature-attributable mortality in Europe: a time series analysis of 147 contiguous regions in 16 countries. eng. *The Lancet. Planetary Health* **5,** e446–e454. ISSN: 2542-5196 (July 2021).

22. Peng Roger D. *et al.* Toward a Quantitative Estimate of Future Heat Wave Mortality under Global Climate Change. *Environmental Health Perspectives* **119,** 701–706. https://ehp.niehs.nih.gov/doi/full/10.1289/ehp.1002430 (2020) (May 2011).

23. Petkova, E., Horton, R., Bader, D. & Kinney, P. Projected Heat-Related Mortality in the U.S. Urban Northeast. en. *International Journal of Environmental Research and Public Health* **10,** 6734–6747. ISSN: 1660-4601. http://www.mdpi.com/1660-4601/10/12/6734 (2020) (Dec. 2013).

24. Schwartz, J. D. *et al.* Projections of temperature-attributable premature deaths in 209 U.S. cities using a cluster-based Poisson approach. en. *Environmental Health* **14,** 85. ISSN: 1476-069X. http://ehjournal.biomedcentral.com/articles/10.1186/s12940-015-0071-2 (2020) (Dec. 2015).

25. Shindell, D. *et al.* The Effects of Heat Exposure on Human Mortality Throughout the United States. en. *GeoHealth* **4.** ISSN: 2471-1403, 2471-1403. https://onlinelibrary.wiley.com/doi/10.1029/2019GH000234 (2021) (2020).

26. Yang, J. *et al.* Projecting heat-related excess mortality under climate change scenarios in China. en. *Nature Communications* **12,** 1039. ISSN: 2041-1723. http://www.nature.com/articles/s41467-021-21305-1 (2021) (Dec. 2021).

27. Zhang, B., Li, G., Ma, Y. & Pan, X. Projection of temperature-related mortality due to cardiovascular disease in beijing under different climate change, population, and adaptation scenarios. en. *Environmental Research* **162,** 152–159. ISSN: 00139351. https://linkinghub.elsevier.com/retrieve/pii/S001393511731770X (2020) (2018).

28. Jáuregui-Díaz, J. A., Sánchez, M. d. J. Á. & Cabañas, R. T. Cambios en la Mortalidad por Eventos Climáticos Extremos en México entre el 2000 y 2015. *Revista de Estudios Latinoamericanos sobre Reducción del Riesgo de Desastres REDER* **4,** 80–94 (2020).

29. Li, T. *et al.* Aging Will Amplify the Heat-related Mortality Risk under a Changing Climate: Projection for the Elderly in Beijing, China. en. *Scientific Reports* **6,** 28161. ISSN: 2045-2322. http://www.nature.com/articles/srep28161 (2020) (June 2016).

30. Mora, C. *et al.* Global risk of deadly heat. en. *Nature Climate Change* **7,** 501–506. ISSN: 1758-6798. https://www.nature.com/articles/nclimate3322 (2019) (July 2017).

31. Armstrong, B. *et al.* The role of humidity in associations of high temperature with mortality: a multicountry, multicity study. *Environmental health perspectives* **127,** 097007 (2019).

32. Raymond, C., Matthews, T. & Horton, R. M. The emergence of heat and humidity too severe for human tolerance. *Science Advances* **6,** eaaw1838 (2020).

33. Sherwood, S. C. & Huber, M. An adaptability limit to climate change due to heat stress. *Proceedings of the National Academy of Sciences* **107,** 9552–9555 (2010).

34. Vecellio, D. J., Wolf, S. T., Cottle, R. M. & Kenney, W. L. Evaluating the 35°C wet-bulb temperature adaptability threshold for young, healthy subjects (PSU HEAT Project). *Journal of Applied Physiology* **132.** Publisher: American Physiological Society, 340–345. ISSN: 8750-7587. https://journals.physiology.org/doi/full/10.1152/japplphysiol.00738.2021 (2023) (Feb. 2022).

35. Vanos, J. *et al.* A physiological approach for assessing human survivability and liveability to heat in a changing climate. en. *Nature Communications* **14,** 7653. ISSN: 2041-1723. https://www.nature.com/articles/s41467-023-43121-5 (2024) (Nov. 2023).

36. Baldwin, J. W. *et al.* Humidity's Role in Heat-Related Health Outcomes: A Heated Debate. en. *Environmental Health Perspectives* **131,** 055001. ISSN: 0091-6765, 1552-9924. https://ehp.niehs.nih.gov/doi/10.1289/EHP11807 (2023) (May 2023).

37. Havenith, G. & Fiala, D. Thermal indices and thermophysiological modeling for heat stress. *Comprehensive Physiology* **6.** Publisher: Wiley Online Library, 255–302 (2011).

38. Buzan, J. R. & Huber, M. Moist Heat Stress on a Hotter Earth. en, 35 (2020).

39. Parsons, K. *Human thermal environments: the effects of hot, moderate, and cold environments on human health, comfort, and performance* (CRC press, 2014).

40. Steadman, R. G. The assessment of sultriness. Part I: A temperature-humidity index based on human physiology and clothing science. *Journal of Applied Meteorology and Climatology* **18,** 861–873 (1979).

41. Ebi, K. L. *et al.* Hot weather and heat extremes: health risks. *Lancet* **398,** 698–708 (2021).

42. Davies-Jones, R. An Efficient and Accurate Method for Computing the Wet-Bulb Temperature along Pseudoadiabats. en. *Monthly Weather Review* **136,** 2764–2785. ISSN: 1520-0493, 0027-0644. http://journals.ametsoc.org/doi/10.1175/2007MWR2224.1 (2023) (July 2008).

43. Schwartz, J. Harvesting and long term exposure effects in the relation between air pollution and mortality. *American Journal of Epidemiology* **151,** 440–448 (2000).

44. Thrasher, B., Maurer, E. P., McKellar, C. & Duffy, P. B. Bias correcting climate model simulated daily temperature extremes with quantile mapping. *Hydrology and Earth System Sciences* **16,** 3309–3314 (2012).

45. Riahi, K. *et al.* The Shared Socioeconomic Pathways and their energy, land use, and greenhouse gas emissions implications: An overview. *Global environmental change* **42,** 153–168 (2017).

46. Dunn, R. J. H., Willett, K. M., Parker, D. E. & Mitchell, L. Expanding HadISD: quality-controlled, sub-daily station data from 1931. *Geoscientific Instrumentation, Methods and Data Systems* **5,** 473–491. https://gi.copernicus.org/articles/5/473/2016/ (2016).

47. Muñoz-Sabater, J. *et al.* ERA5-Land: a state-of-the-art global reanalysis dataset for land applications. *Earth System Science Data* **13,** 4349–4383. https://essd.copernicus.org/articles/13/4349/2021/ (2021).

48. Raymond, C. *et al.* Regional and elevational patterns of extreme heat stress change in the US. *Environmental Research Letters* **17,** 064046 (2022).

49. Cohen, F. & Dechezleprêtre, A. Mortality, temperature, and public health provision: evidence from Mexico. *American Economic Journal: Economic Policy* **14,** 161–192 (2022).

50. Powis, C. M. *et al.* Observational and model evidence together support wide-spread exposure to noncompensable heat under continued global warming. *Science Advances* **9.** Publisher: American Association for the Advancement of Science, eadg9297. https://www.science.org/doi/10.1126/sciadv.adg9297 (2023) (Sept. 2023).

51. Wu, Y. *et al.* Global, regional, and national burden of mortality associated with short-term temperature variability from 2000–19: a three-stage modelling study. *The Lancet Planetary Health* **6,** e410–e421. ISSN: 2542-5196. https://www.sciencedirect.com/science/article/pii/S2542519622000730 (2023) (May 2022).

52. EPA. *Supplementary Material for the Regulatory Impact Analysis for the Supplemental Proposed Rulemaking, "Standards of Performance for New, Reconstructed, and Modified Sources and Emissions Guidelines for Existing Sources: Oil and Natural Gas Sector Climate Review"* Sept. 2022. https://t.co/QllVBWDGmL.

53. Rennert, K. *et al.* Comprehensive evidence implies a higher social cost of CO2. en. *Nature* **610.** Number: 7933 Publisher: Nature Publishing Group, 687–692. ISSN: 1476-4687. https://www.nature.com/articles/s41586-022-05224-9 (2023) (Oct. 2022).

54. Vassilieff, N., Rosencher, N., Sessler, D. I. & Conseiller, C. Shivering threshold during spinal anesthesia is reduced in elderly patients. *The Journal of the American Society of Anesthesiologists* **83,** 1162–1166 (1995).

55. Saely, C. H., Geiger, K. & Drexel, H. Brown versus white adipose tissue: a mini-review. *Gerontology* **58,** 15–23 (2011).

56. Meade, R. D. *et al.* Physiological factors characterizing heat-vulnerable older adults: a narrative review. *Environment international* **144,** 105909 (2020).

57. Zanobetti, A., O'Neill, M. S., Gronlund, C. J. & Schwartz, J. D. Susceptibility to mortality in weather extremes: effect modification by personal and small area characteristics in a multi-city case-only analysis. *Epidemiology (Cambridge, Mass.)* **24,** 809 (2013).

58. Brown, D. J., Brugger, H., Boyd, J. & Paal, P. Accidental hypothermia. *New England Journal of Medicine* **367,** 1930–1938 (2012).

59. Kovats, R. S. & Hajat, S. Heat stress and public health: a critical review. *Annu. Rev. Public Health* **29,** 41–55 (2008).

60. Leigh-Hunt, N. *et al.* An overview of systematic reviews on the public health consequences of social isolation and loneliness. *Public health* **152,** 157–171 (2017).

61. Gertler, P. J., Shelef, O., Wolfram, C. D. & Fuchs, A. The demand for energy-using assets among the world's rising middle classes. *American Economic Review* **106,** 1366–1401 (2016).

62. Soriano-Hernandez, P., Mejia-Montero, A. & van der Horst, D. Characterisation of energy poverty in Mexico using energy justice and econophysics. *Energy for Sustainable Development* **71,** 200–211 (2022).

63. Falk, B. & Dotan, R. Children's thermoregulation during exercise in the heat—a revisit. *Applied Physiology, Nutrition, and Metabolism* **33,** 420–427 (2008).

64. Xu, Z. *et al.* Impact of ambient temperature on children's health: A systematic review. en. *Environmental Research* **117,** 120–131. ISSN: 00139351. `https://linkinghub.elsevier.com/retrieve/pii/S0013935112001983` (2022) (Aug. 2012).

65. Brown, J. J., Pascual, M., Wimberly, M. C., Johnson, L. R. & Murdock, C. C. Humidity–The overlooked variable in the thermal biology of mosquito-borne disease. *Ecology Letters* (2023).

66. Graff Zivin, J. & Shrader, J. Temperature extremes, health, and human capital. *The Future of Children,* 31–50 (2016).

67. Kjellström, T., Maître, N., Saget, C., Otto, M. & Karimova, T. *Working on a warmer planet: The impact of heat stress on labour productivity and decent work* (ILO, 2019).

68. Gaigbe-Togbe, V., Bassarsky, L., Gu, D., Spoorenberg, T. & Zeifman, L. World population prospects 2022. *Department of Economic and Social Affairs, Population Division: New York, NY, USA* (2022).

69. For Economic, U. N. D. & Affairs, S. *World Population Prospects 2022: Summary of results* (UN, 2023).

70. Fischer, E. M. & Knutti, R. Robust projections of combined humidity and temperature extremes. en. *Nature Climate Change* **3,** 126–130. ISSN: 1758-678X, 1758-6798. https://www.nature.com/articles/nclimate1682 (2023) (Feb. 2013).

71. Yuan, J., Stein, M. L. & Kopp, R. E. The evolving distribution of relative humidity conditional upon daily maximum temperature in a warming climate. *Journal of Geophysical Research: Atmospheres* **125,** e2019JD032100 (2020).

72. Buzan, J. R., Oleson, K. & Huber, M. Implementation and comparison of a suite of heat stress metrics within the Community Land Model version 4.5. en. *Geoscientific Model Development* **8,** 151–170. ISSN: 1991-9603. https://gmd.copernicus.org/articles/8/151/2015/ (2024) (Feb. 2015).

73. Barreca, A., Clay, K., Deschenes, O., Greenstone, M. & Shapiro, J. S. Adapting to climate change: The remarkable decline in the US temperature-mortality relationship over the twentieth century. *Journal of Political Economy* **124,** 105–159 (2016).

74. Shrader, J., Bakkensen, L. & Lemoine, D. *Fatal Errors: The Mortality Value of Accurate Weather Forecasts* 2023.

75. Geruso, M. & Spears, D. Heat, Humidity, and Infant Mortality in the Developing World. *NBER Working Paper* **No. 24870,** 31. http://www.nber.org/papers/w24870.ack (2018) (2018).

76. Lab, F. C. & for International Earth Science Information Network – CIESIN – Columbia University, C. *High Resolution Settlement Layer (HRSL)* Source imagery for HRSL © 2016 DigitalGlobe. 2016.

77. Harrell, F. E. *Regression Modeling Strategies: With Applications to Linear Models, Logistic and Ordinal Regression, and Survival Analysis* ISBN: 9783319194257. http://dx.doi.org/10.1007/978-3-319-19425-7 (Springer International Publishing, 2015).

78. Gasparrini, A. Distributed lag linear and non-linear models in R: the package dlnm. *Journal of statistical software* **43,** 1 (2011).

493 79. Dong, J., Bronniman, S., Hu, T., Liu, Y. & Peng, J. GSDM-WBT: Global station-based daily
494 maximum wet-bulb temperature data for 1981-2020. *Earth System Science Data* (2022).

495 80. Sims, K. *et al. LandScan Global 2022* `https://landscan.ornl.gov` (2023).

A Supplementary Materials

A.1 Data

A.1.1 Mortality, population, and life expectancy data

We collect mortality data from the Subsistema de Información Demográfica y Social of Mexico's Instituto Nacional de Estadística y Geografía. This data contains records of all recorded mortality events in Mexico since 1990. Our data period begins in 1998, when this mortality microdata first began to carry information about the day and municipality of each mortality event. Our data period ends in 2019, after which some death records are still preliminary and the COVID-19 pandemic exerts a large influence on behavior and mortality. Between 1998 and 2019, we observe in this data 13,426,931 deaths. The World Bank estimates that Mexico's all-cause crude mortality rate is around 6 deaths per 1000 people per year. Relative to a population of around 110 million during this period, this would imply total deaths of 14.5 million during our data period, giving us confidence that these mortality records are relatively complete. Across the data, each recorded mortality event also contains information on the cause of the individual's death as well as the individual's sex, education level, occupation, place of residence, and age at death. We drop death records that are missing information on the day of death, the individual's age at death, or the death location. We also drop death records reporting deaths that occurred outside of Mexico. These dropped records represent less than 0.92% of the data.

Data on administrative unit population, which is used to determine mortality rates and regression weights, is collected from IPUMS International, which consolidates and harmonizes census data for Mexico. Our study uses data from the 1990, 2000, and 2010 Mexican censuses, as well as the 2015 Intercensal Survey. Population for each administrative unit is assumed to grow at a constant rate between observations, and population growth between the 2010 Census and 2015 Intercensal Survey is assumed to remain constant through the end of our data in 2019.

Across both mortality and population data, we account for 67 municipal boundary changes occurring between 1998 and 2019 by assigning values reported for modified units to an aggregate set of 2,402 municipal units that is stable across all years of our study. We also aggregate deaths

and population across age groups: age (1) less than 5, (2) at least 5 and less than 18, (3) at least 18 and less than 35, (4) at least 35 and less than 50, (5) at least 50 and less than 70, (6) at least 70.

In this study, we sometimes report values in terms of lost life years. Our estimates for the age-dependent number of remaining life years at time of death for the average person in each age group come from the United Nations 2022 World Population Prospects, with expected remaining life years for an age group calculated as a weighted mean of the expected remaining life years of cohorts in each age classification across all sample years (i.e., expected remaining life years of those less than 5 is estimated as the expected remaining life years of age cohorts aged 0, 1, 2, 3, and 4 across every year from 1998 to 2019, weighted by the population size of each cohort). The resulting scalars are not particularly sensitive to the aggregation procedure, as potential remaining life years did not change markedly for any age group in Mexico during our data period. The scalars range from 73.32 expected remaining life years for the under-5 age group to 9.91 expected remaining life years for the 70+ age group.

A.1.2 Weather data

Our observational weather dataset is collected from the UK Met Office Hadley Centre's Integrated Surface Dataset, which consolidates observations from a global network of weather stations but performs various quality control adjustments to ensure the consistency of observations over time. The resulting dataset we use contains a set of weather metrics recorded at a sub-daily frequency (some stations report weather at an hourly frequency, but many report at three- or six-hour intervals). A map of the stations reporting data used in our analysis is shown in Figure S14.

Extreme wet-bulb temperature events at thresholds sufficiently high to impact human health may be short in duration and tightly spatially constrained [32]. Accordingly, recent literature has suggested that the spatial and temporal smoothing involved in the creation of reanalysis products often leads to underestimations of the intensity of extreme humid heat events compared to observational datasets [32]. While [75], for instance, use the Princeton Meteorological Forcing Dataset which is based on reanalysis from NCEP/NCAR and the CRU with a spatial resolution of 0.25

degrees, we find that even reanalysis products with over six-times higher resolution (ERA5-Land) are unable to capture humid heat extremes. This is a known limitation of reanalysis products, though recent work has argued that reanalysis products may be suitable for studies exploring the relationship between temperature and mortality. This is not the case when such studies consider humidity, which varies more over space. Indeed, many of the most extreme humid heat events arise from intrusions of moist air above very warm seas into coastal cities on very hot days, a point emphasized in [32].

We first use the method described in [42] to approximate wet-bulb temperature from dry-bulb temperature, surface pressure, and dew point temperature at each station location. As our method requires matching station temperature records to administrative units, we then perform an adjustment to fill missing hourly dry-bulb and wet-bulb temperature observations by leveraging distributional information from nearby non-missing stations. To avoid filling missing data for stations that report infrequently or for which we do not have a sufficiently diverse historical record, we first drop from our data all stations that report fewer than 10,000 observations during the period from 1990 to 2019 (roughly 3% of hours) as well as stations that do not report more than 1000 observations across at least 10 years. For each of the remaining stations, we then determine an empirical cumulative distribution function for all non-missing observations. Next, if the data does not contain an observation for a given station at a particular hour, we determine a likely quantile for this observation using an inverse squared geodesic distance-weighted mean of all stations in Mexico that are reporting values at that hour. We then fill the missing value using the temperature at that quantile for that station. Said differently, if a station is missing data at a particular hour and nearby non-missing temperatures are on average at their 90^{th} percentile, we set the missing value to the 90^{th} percentile of the historical readings for that station. This method is deployed in the dataset here.

We obtain daily mean dry-bulb and wet-bulb temperatures by calculating the average of the daily minima and maxima of each metric at each station. We next determine the geodesic distance between each station and the population-weighted centroid of each administrative unit and map temperature observations to administrative units by taking the inverse squared distance-weighted

mean of each temperature metric for the five nearest stations (see Figure S14 for the locations of stations used in the study). This method is similar to other papers studying temperature effects on mortality using weather station data [73]. To determine the population-weighted centroid of each administrative unit, we use Meta's High-Resolution Population Density Maps [76]. To ensure that we are using representative weather station data to estimate exposure, we omit from our analysis municipalities whose population center of mass is more than 50 kilometers from the nearest weather station. These municipalities represent 24.83% of Mexico's population as of the date of the 2010 Census.

Precipitation data is collected from the European Centre for Medium-range Weather Forecasting Reanalysis 5 - Land (ERA5-Land) dataset (and included as a control to avoid confounding effects). Using Google Earth Engine, a daily total precipitation measure is calculated by taking a sum over the hourly values across each day at each grid cell and then taking a spatial average over each administrative unit, weighting by a gridded estimate of the time-varying distribution of population (Gridded Population of the World v4, revision 11).

A.2 Statistical model

Estimates of the effect of temperature on mortality come from fitting a mortality response function following [1]. The outcome variables—daily, location-specific mortality rates for each age group—are modeled as dynamic functions of temperature and precipitation, with additional controls for location-specific, time-varying, and seasonal confounders. Formally,

$$y_{ait} = f_a(x_{it}, \ldots, x_{it-30};\ \mathbf{B}_a) + g_a(p_{it}, \ldots, p_{it-30};\ \mathbf{\Gamma}_a) \tag{S-1}$$

$$+ \rho_{at} + \delta_{ai} \times \text{year}_t + \theta_{as} \times h(\text{doy}_t;\ \xi_a) + \varepsilon_{ait} \tag{S-2}$$

where y_{ait} is the mortality rate (deaths per 100,000 people) in municipality i on date t and age group $a \in \{< 5, 5\text{–}17, 18\text{–}34, 35\text{–}49, 50\text{–}69, > 70\}$. Separate models are fit for each age group.

The main right-hand-side variable is daily average temperature—either dry-bulb or wet-bulb depending on the specification—generically denoted x_{it} in the above equation. The relationship

between temperature and mortality is allowed to be nonlinear and dynamic, as captured by the function $f_a(x_{it}, \ldots, x_{it-30};\ \mathbf{B}_a)$, with $\mathbf{B}_a$ denoting the matrix of unknown coefficients to be estimated. This function transforms temperature observations along two dimensions. In the temperature dimension, the function is a natural cubic spline over daily temperature with knots at the 10^{th}, 50^{th}, and 90^{th} percentiles [77]. (For dry-bulb temperature, these knots are at approximately 14.92, 20.63, and 27.51°C; for wet-bulb temperature, they are at approximately 9.14, 15.37, and 22.80°C.) Across 31 days of distributed lags, the function is a b-spline with knots spaced equally, in log terms, across the lag period (at roughly 1, 3, and 10 days). Putting these elements together, fitting the model generates estimates of the effect of temperature on mortality at each point across the distribution of temperatures and for each of 31 days starting with with the initial day of the temperature realization. From these estimates, we calculate and report the 30-day cumulative effect of temperature on mortality, as depicted in Figure 1.

The other elements of the estimating equation are controls. Daily total precipitation, p_{it} is included in a similar way to temperature, with the cumulative effect estimated using a b-spline distributed lag. The effect of precipitation is modeled flexibly using 0^{th}-order splines (i.e., bins) for precipitation below the 80^{th} percentile (roughly zero precipitation), between the 80^{th} and 90^{th} percentiles, between the 90^{th} and 95^{th} percentiles, between the 95^{th} and 98^{th} percentiles, between the 98^{th} and 99.5^{th} percentiles, and above the 99.5^{th} percentile (the levels of these breaks are approximately 5.31, 10.5, 15.6, 23.7, and 45.3 mm/day). Other confounders are accounted for using fixed effects, in some cases interacted with continuous controls. These controls are: date of sample fixed effects, ρ_{at}, to account for national temporal patterns, holidays, day-of-week effects, and other time-series confounders; a municipality-by-year fixed effect, $\delta_{ai} \times \text{year}_t$, to account for location-specific fixed factors such as topography, governance, and differences in access to healthcare or mortality reporting as well as secular changes in mortality rates and climate; and a state-level fixed effect, θ_{as}, interacted with a six-knot natural cubic spline over day-of-year, $h(\text{doy}_t;\ \xi_a)$, to account for state-level seasonal patterns. The term ϵ_{ait} is the remaining error term which we assume to be uncorrelated with daily temperature.

The regression is weighted by the daily municipality population (linearly interpolated from an-

nual population counts). Standard errors are clustered at the state level to account for spatial autocovariances at the subnational level while maintaining robustness to arbitrary temporal correlation patterns ($N = 32$).

Throughout, such as when we distinguish deaths from heat from those from cold or when we report the total number of temperature-related deaths, we are identifying these values relative to an age group-specific optimal temperature, or minimum mortality temperature (MMT). While semantically the MMT is simply the temperature at which mortality is minimized, the flexible functional form we use to determine the relationship between temperature and mortality leads to a corner solution for the global MMT for some age groups. To prevent this, we instead define the MMT conditionally as the temperature between the 1^{st} and 99^{th} percentiles of age group-specific temperature exposure at which mortality is minimized [1]. As we discuss in the main body text, MMT varies considerably by age, generally rising throughout the lifespan.

Models are fit using R software version 4.2.2 and the `dlnm` package version 2.4.7 [78].

A.3 Projections

In addition to identifying historical relationships between wet-bulb temperature and mortality, we make projections of the impact of climate change on these relationships through the end of the century. The projections focus on the effect of changes in dry and moist heat, holding all other aspects of the system fixed. To make temperature-related mortality projections, we apply the age-specific exposure-response functions estimated from our statistical model to the future temperature projections described above, and assume that these functions will continue to hold in the future, as in [10]. Thus, we hold the severity of the effect of wet- and dry-bulb temperature on mortality and the demographic characteristics of the country fixed, then change the levels of experienced wet- and dry-bulb temperatures. This method facilitates comparison between the effect of current and future climates.

For the climate projections, and again motivated by the need to capture fine scale spatial variability in dry and humid heat, we select the NASA Earth exchange Global Daily Downscaled Projections (NEX-GDDP) dataset, a product statistically downscaled from Coupled Model Inter-

comparison Project Phase 6 (CMIP6) General Circulation Models (GCMs), as the underlying data for our projections. This downscaled product provides daily data at a spatial resolution of 0.25 degrees, significantly more fine than the underlying CMIP6 models which primarily have a resolution of approximately 1 degree. In order to apply the statistical model to various future periods and measure the potential changes in the differential impacts of humid and dry heat on human health, the variables necessary for projections include daily mean dry-bulb temperature, daily mean specific humidity, daily mean pressure, and daily total precipitation. Because the NEX-GDDP dataset does not supply daily mean pressure data, we use an elevation-based approximation at each point. While this method ignores the wet-bulb temperature effects of temporal pressure fluctuations, the resultant bias is no more than approximately 0.25°C [79]. Twenty six models are selected based on their inclusion of these variables. We perform projections for one ensemble member using representative concentration pathways (RCPs) from four Shared Socioeconomic Pathway (SSP) scenarios, namely SSPs 1-2.6, 2-4.5, 3-7.0, and 5-8.5.

We then use percentile mapping to generate synthetic time series for each meteorological variable (dry-bulb temperature and precipitation as downloaded directly from NEX-GDDP; wet-bulb temperature calculated from NEX-GDDP data as described above) during an end-of-century period. Within each model and SSP-RCP scenario, data from the historical and future periods are binned into 1 percentile bins (e.g., 1^{st} percentile, 2^{nd} percentile, ..., 99^{th} percentile). The delta change for each variable in these percentiles is computed between the historical period and future periods. These percentile-specific change factors are then applied to the corresponding percentile days in the observational station data. This approach retains any seasonality and internal variability recorded in the observational historical period, is flexible, and allows for the mean and higher moments of the future distribution of temperatures to be different than what was observed historically.

To ensure comparability between average annual outcomes in the past and in projections, we calculate past average annual outcomes using only exposures from 1998–2014. This period represents the overlap between our mortality data (1998–2019) and the historical period for NEX-GDDP models (1950–2015). The mid-century (2043–2059) and end-of-century (2083–2099) periods are defined to be the same length as this past period, 17 years. Throughout, we use the term "histor-

ical" to refer to the period 1998–2014; when discussing the data period over which we resolve our exposure–response functions (1998–2019), we use the term "sample period."

A.4 Additional Figures

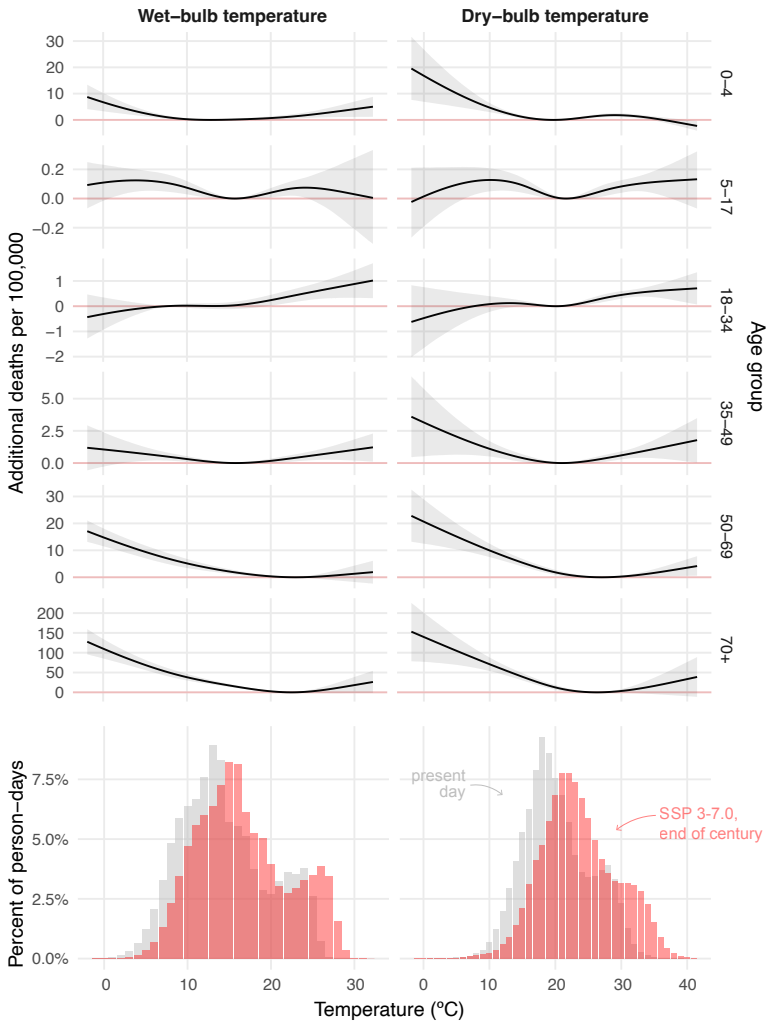


Figure S1: Relationships between mortality and exposure to wet- and dry-bulb temperature by age group in Mexico
This figure mirrors Figure 1, but expresses outcomes as absolute changes in deaths and adds a column for dry-bulb temperature. The top panels show the additional effects of 100,000 person-days of exposure to the indicated daily average wet- and dry-bulb temperatures (x-axis) on mortality (y-axis); exposure and mortality are in terms of the indicated age group. Bands around each function indicate 95% confidence intervals. The bottom panel shows the distribution of daily average wet- and dry-bulb temperatures in Mexico throughout our sample period as well as the ensemble mean of projected temperatures under the SSP 3-7.0 emission scenario at the end of the century (2083–2099); we impose no change in population distribution or size.

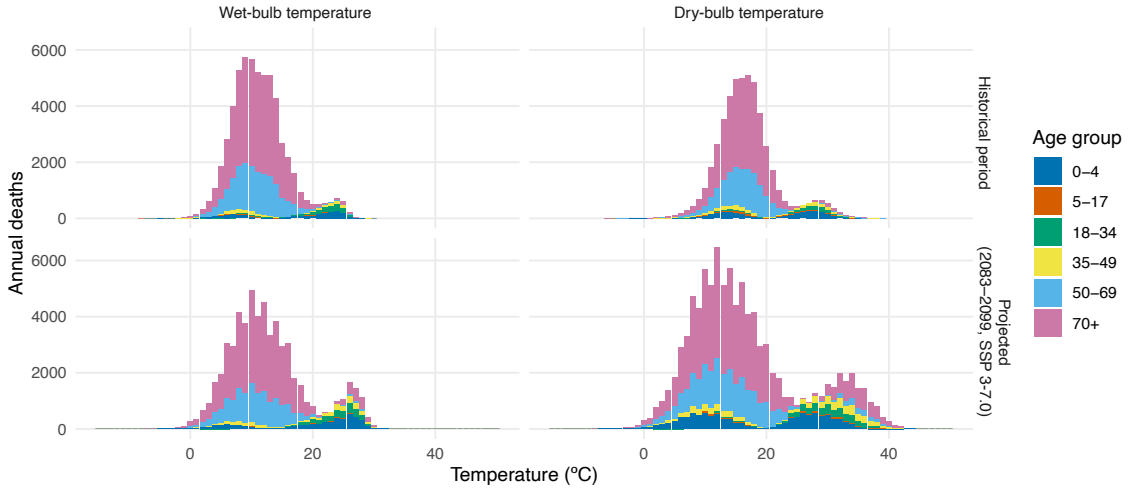


Figure S2: Historical and projected annual temperature-related deaths in Mexico for degree bins of wet- and dry-bulb temperature
This figure mirrors Figure 2, but adds a column for dry-bulb temperature. The panels show average annual temperature-related deaths resulting from exposure to days with the average wet- or dry-bulb temperatures shown on the x-axis during the historical period (top panels) and at the end of the century (2083–2099) under the SSP 3-7.0 emission scenario (bottom panels) across six age groups in Mexico. The figure shows mean projected deaths; see Figure S3 for projections with uncertainty.

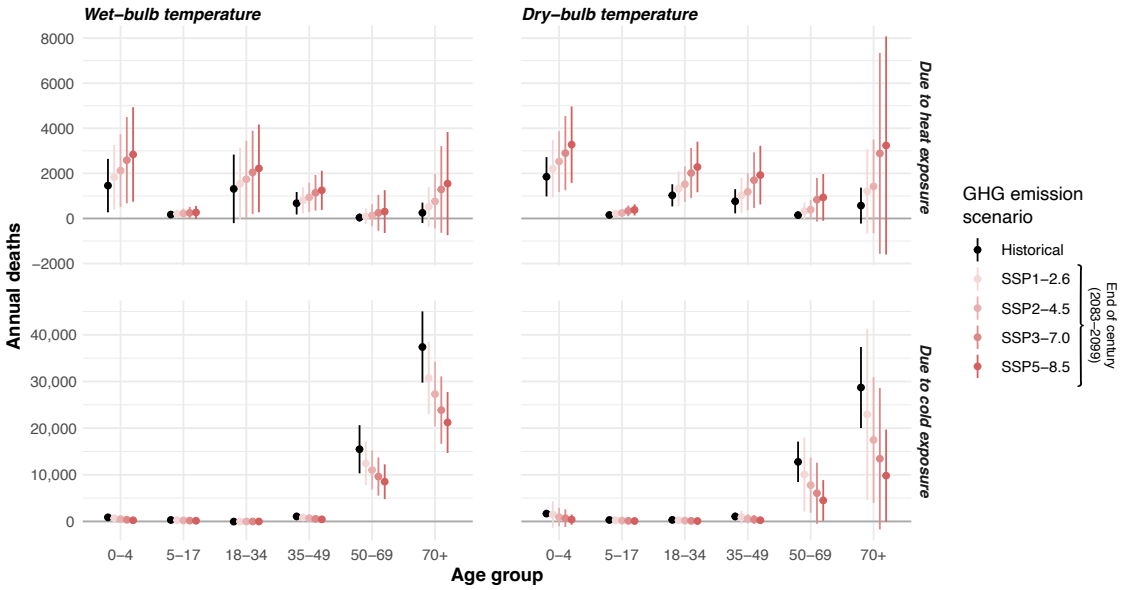


Figure S3: Historical and projected annual deaths due to heat and cold exposure by age group for wet- and dry-bulb temperature

This figure mirrors Figure 3, but adds a column for dry-bulb temperature. The figure depicts the annual number of deaths attributed to heat and cold exposure in Mexico historically and under temperatures prevailing at the end of the century in four greenhouse gas emission scenarios. Top panels indicate values for heat exposure, whereas bottom panels indicate values for cold exposure. Estimates using wet-bulb temperature are shown in the left panels, whereas those derived using dry-bulb temperature are shown in the right panels. Whiskers above and below each estimate depict 95% confidence intervals net of both econometric and climate uncertainty. Note that the range of the y-axis in the bottom panels is roughly five times the range of the y-axis in the top panels.

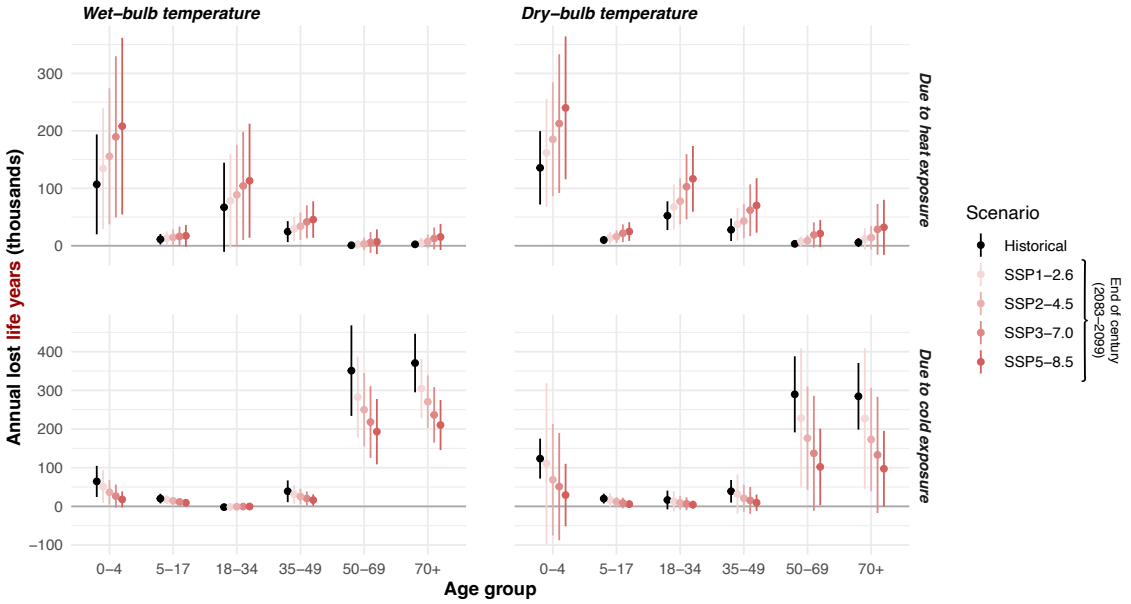


Figure S4: Historical and projected annual lost life years due to heat and cold exposure by age group for wet- and dry-bulb temperature

This figure mirrors Figure 4, but with the outcome as lost life years, rather than deaths. Potential remaining life years are taken from the UN World Population Prospects 2022, and are aggregated to time-invariant age group values by taking a population-weighted average across single age bins and years. The figure depicts the annual number of lost life years attributed to heat and cold exposure in Mexico historically and under temperatures prevailing at the end of the century in four greenhouse gas emission scenarios. Top panels indicate values for heat exposure, whereas bottom panels indicate values for cold exposure. Estimates using wet-bulb temperature are shown in the left panels, whereas those derived using dry-bulb temperature are shown in the right panels. Whiskers above and below each estimate depict 95% confidence intervals net of both econometric and climate uncertainty.

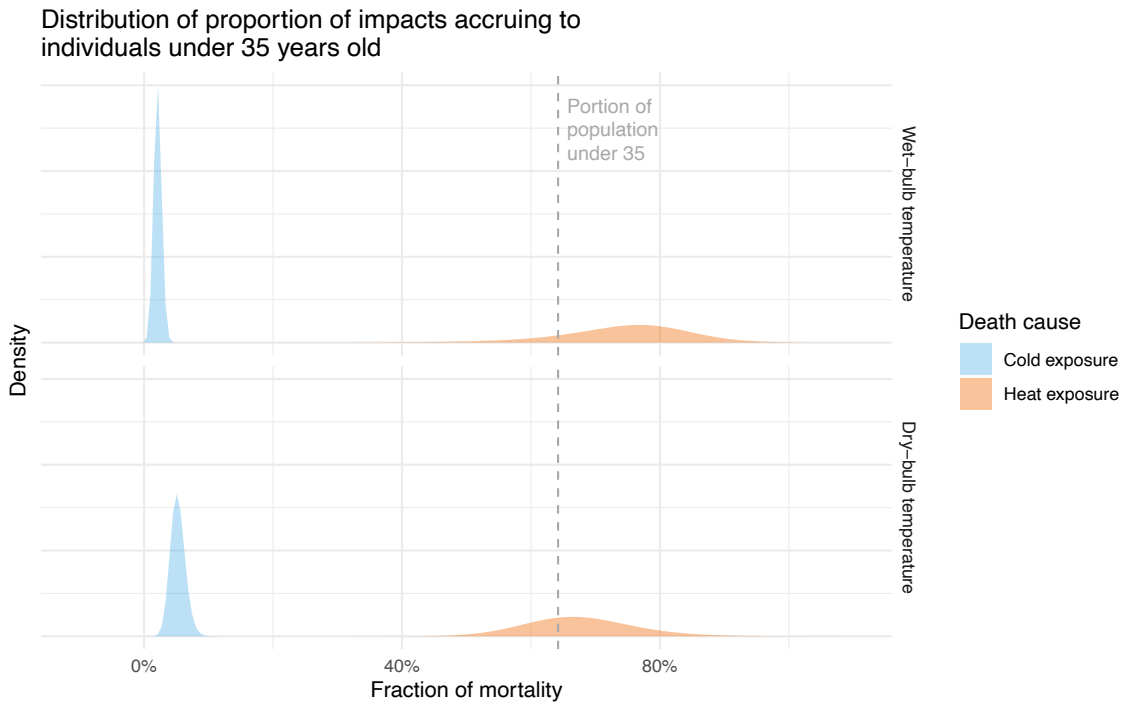


Figure S5: Distribution of estimates of the historical proportion of heat and cold-related deaths occurring to individuals under 35 years old.

Distributions depict the density of bootstrap samples i of $\frac{\text{deaths_under_35}_{i,\text{type}}}{\text{all_deaths}_{i,\text{type}}}$, where the number of samples is 10,000 and type $\in$ {cold-related, heat-related}. Results using wet-bulb temperature are shown in the top panel, whereas results using dry-bulb temperature are shown in the bottom panel. As of the 2010 Census, around 63% of the Mexican population is under 35, a value labeled on the plot with a dashed vertical line.

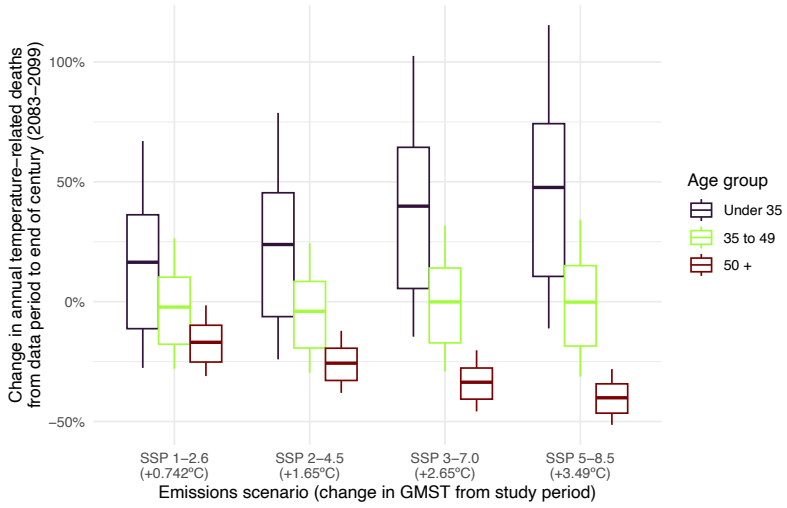


Figure S6: Projected percent change in annual deaths in Mexico under different climate change scenarios using wet-bulb temperature projections
The figure shows the percent change in average annual deaths by end-of-century (2083–2099) relative to the historical period for four different climate scenarios, indicated on the x-axis, and for three different age groups: those under 35 years old, between 35 and 49 years old, and over 50 years old. Box boundaries depict the 25^{th} and 75^{th} percentile of bootstrap estimates, while whiskers depict the 10^{th} and 90^{th} percentiles. The differences in levels is shown in Figure S7.

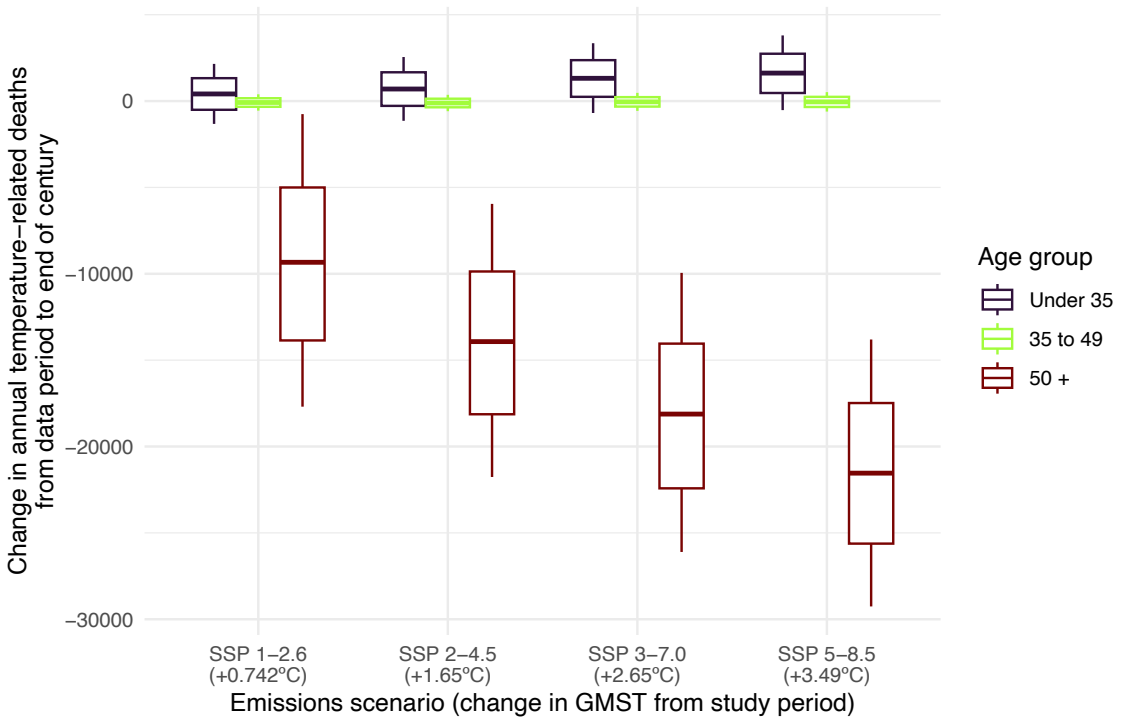


Figure S7: Projected change in annual deaths in Mexico under different climate change scenarios using wet-bulb temperature projections
The figure shows the level of average annual deaths by end-of-century (2083–2099) relative to the historical period for four different climate scenarios, indicated on the x-axis, for three different age groups: those under 35 years old, those between 35 and 49 years old, and those over 50 years old. Box boundaries depict the 25^{th} and 75^{th} percentile of bootstrap estimates, while whiskers depict the 10^{th} and 90^{th} percentiles. Figure S6 shows the same information but in terms of percent change.

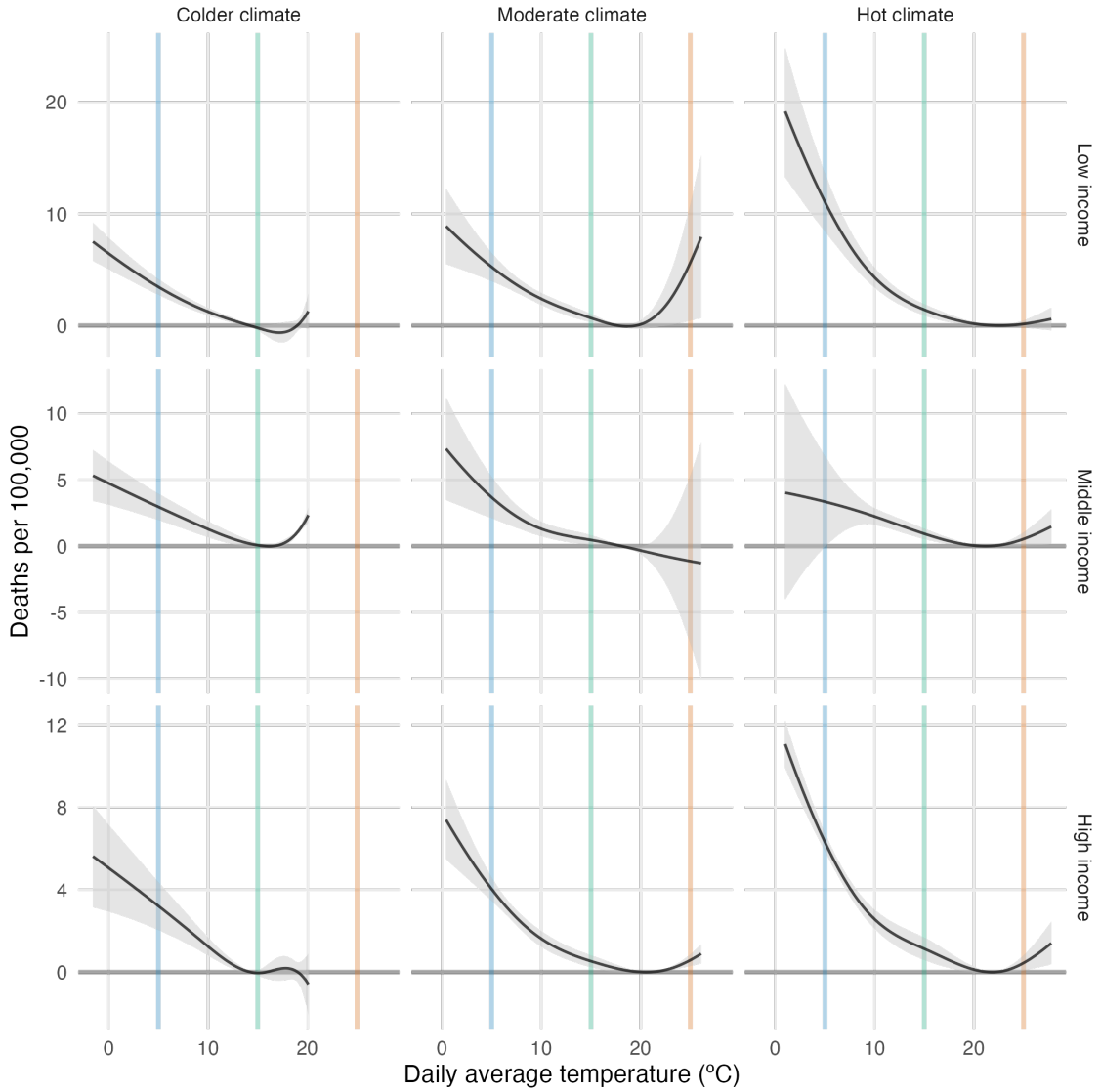


Figure S8: Lag–response relationship when estimating Eq. S-1
Relationship between average daily wet–bulb temperature and additional deaths per 100,000 person–days of exposure by income and climate tercile. Income terciles divide Mexico's municipalities into three roughly equal-population groups by their average earned income as reported by the Mexican census; climate terciles divide Mexico's municipalities into three roughly equal-population groups by their average annual wet-bulb temperature during the data period. Effects are for the overall population (pooled across age groups). Shaded area represents a confidence interval of 95%. Dose–response functions are shown to each tercile's population-weighted 0.01 and 99.99 percentile temperature exposure (colored vertical lines are added at 5, 15, and 25°C to aid visual comparison).

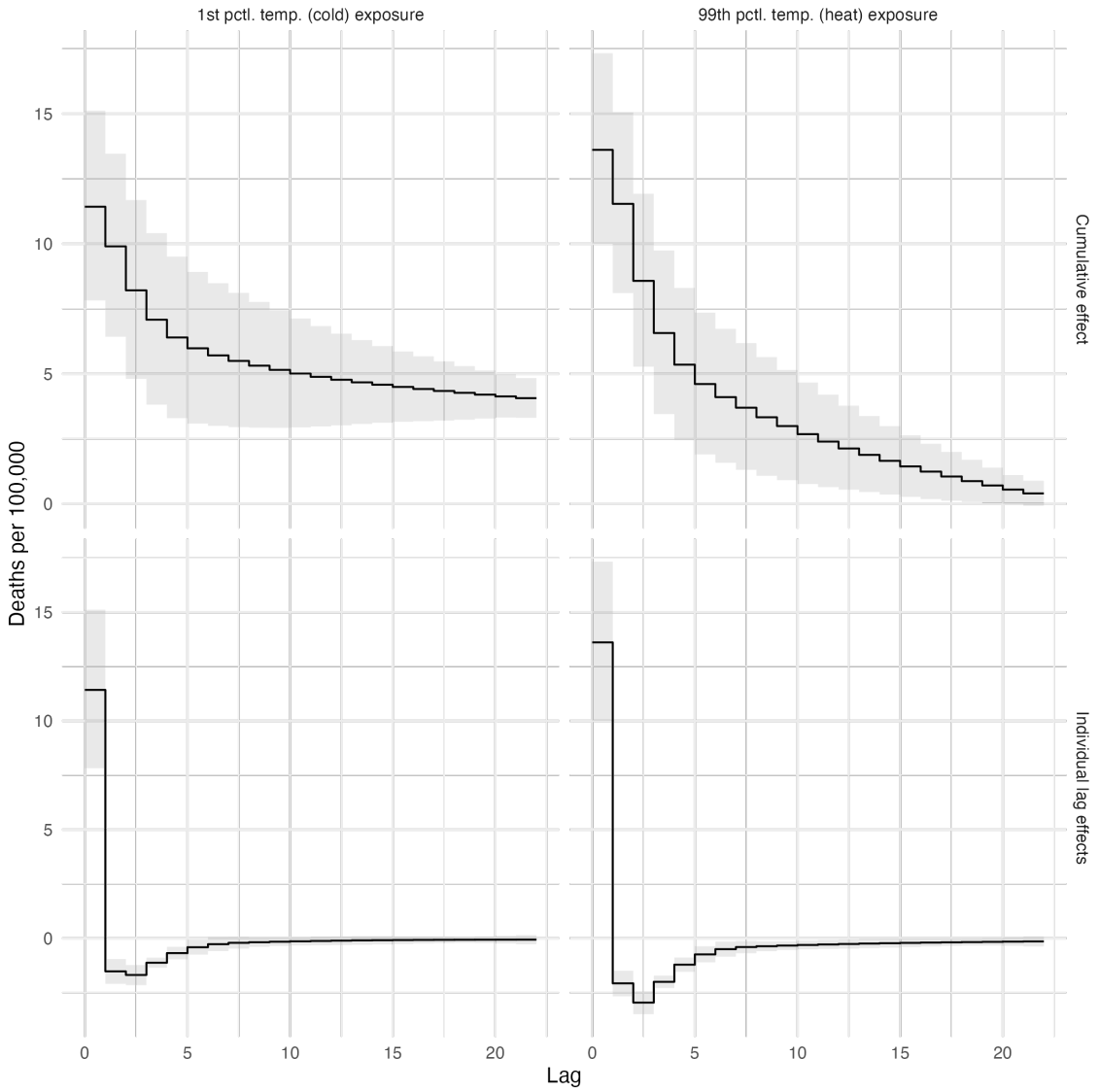


Figure S9: Lag–response relationship when estimating Eq. S-1
Additional deaths per 100,000 person–days of exposure to average daily 1^{st}- (left panels) and 99.9^{th}- (right panels) percentile wet-bulb temperatures (approximately 3.96 and 25.25°C, respectively). Effects are for the overall population (pooled across age groups). Top panels show cumulative effects across the 21-day lag period; bottom panels show the effects at individual lags. Shaded area represents a confidence interval of 95%.

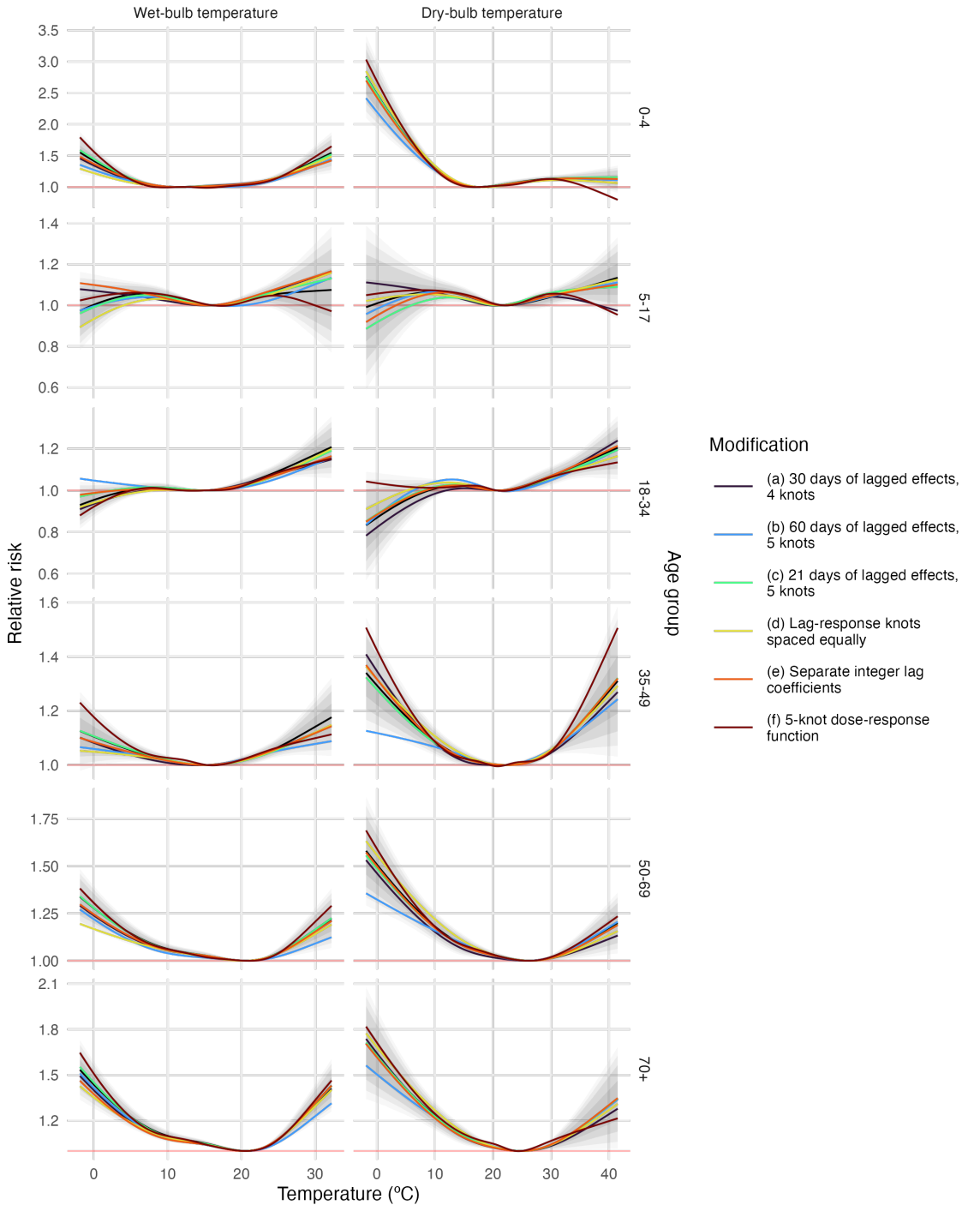


Figure S10: Robustness of results to modifications to Eq. S-1
Estimated relationship between wet- and dry-bulb temperature and relative risk of mortality by age group for alternate model specifications. (a) extends the main model's 21-day lag period to 30 days and adds a single knot to the 3-knot lag–response specification to preserve a similar degree of flexibility in the lag–response function; (b) extends this further to 60 days and adds another knot to the lag–response function. (c) adds two additional knots to the main model's 21-day lag structure, bringing the total number of lag–response function knots to five. (d) changes the placement of the main model's three lag–response knots, placing them equally throughout the lag space instead of spaced logarithmically. (e) includes separate coefficients for each integer lag in the main model's 21-day lag space. (f) changes the specification of the dose–response function, increasing the number of knots from three to five, with placement following [77]. Shaded bands around the main model result indicate 95, 90, 80, and 50% confidence intervals.

Table S1: Additional deaths per 100,000 person–days of exposure to an average daily wet-bulb temperature in the indicated bin. Values were determined by estimating Equation S-1, but with a discretized version of the nonlinear dose–response component of $f_a(\cdot)$. Standard errors are shown in parentheses.

	Age group					
Temperature (°C)	0–4	5–17	18–34	35–49	50–69	70+
<3	2.923	0.057	-0.661	0.315	5.366	49.42
	(0.91)	(0.101)	(0.178)	(0.385)	(1.255)	(9.21)
[3,6)	1.582	0.051	0.142	0.851	4.466	32.834
	(0.504)	(0.041)	(0.077)	(0.194)	(0.83)	(6.13)
[6,9)	0.334	0.063	0.029	0.165	2.352	18.623
	(0.327)	(0.033)	(0.044)	(0.134)	(0.581)	(3.643)
[9,12)	0.124	0.041	0.042	0.217	1.546	10.819
	(0.218)	(0.026)	(0.037)	(0.101)	(0.37)	(2.361)
[12,15)	0.222	0.015	0	0.059	0.932	8.927
	(0.216)	(0.027)	(0)	(0.088)	(0.369)	(2.212)
[15,18)	0	0	0.032	0	0.449	1.946
	(0)	(0)	(0.053)	(0)	(0.286)	(1.353)
[18,21)	0.444	0.024	0.069	0.086	0	0
	(0.208)	(0.022)	(0.067)	(0.09)	(0)	(0)
[21,24)	0.648	0.048	0.218	0.331	0.114	0.804
	(0.22)	(0.024)	(0.071)	(0.114)	(0.227)	(1.062)
[24,27)	1.441	0.058	0.303	0.483	1.174	9.606
	(0.307)	(0.045)	(0.083)	(0.148)	(0.488)	(2.47)
27+	3.392	0.008	1.049	2.061	3.575	41.039
	(0.982)	(0.35)	(1.158)	(1.272)	(2.399)	(8.131)

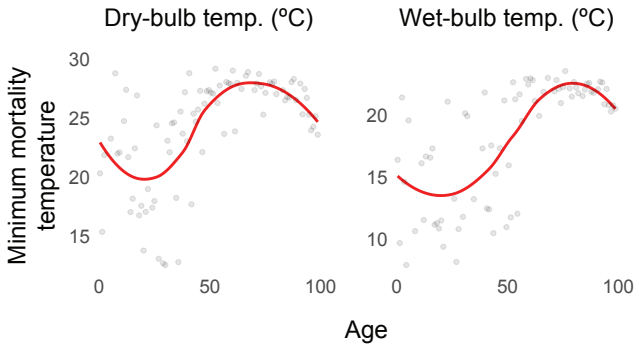


Figure S11: Minimum mortality temperatures across age groups in Mexico
This figure demonstrates the relationship between age and the temperature at which mortality is minimized ("MMT"). A locally-weighted regression line is added to aid in visual inspection, as these parameter estimates are subject to noise. These MMTs are determined by separately estimating Eq. S-1 for each age and temperature metric and determining the temperature at which mortality risk is minimized. MMT decreases from birth to the mid-20s, and then increases substantially with age to around age 70 before flattening and decreasing slightly to age 100. Individuals in their mid-20s have a dry-bulb MMT of 20°C and a wet-bulb MMT of 13°C. Dry-bulb MMT peaks at 28°C at age 70 and wet-bulb MMT peaks at 22°C at age 75.

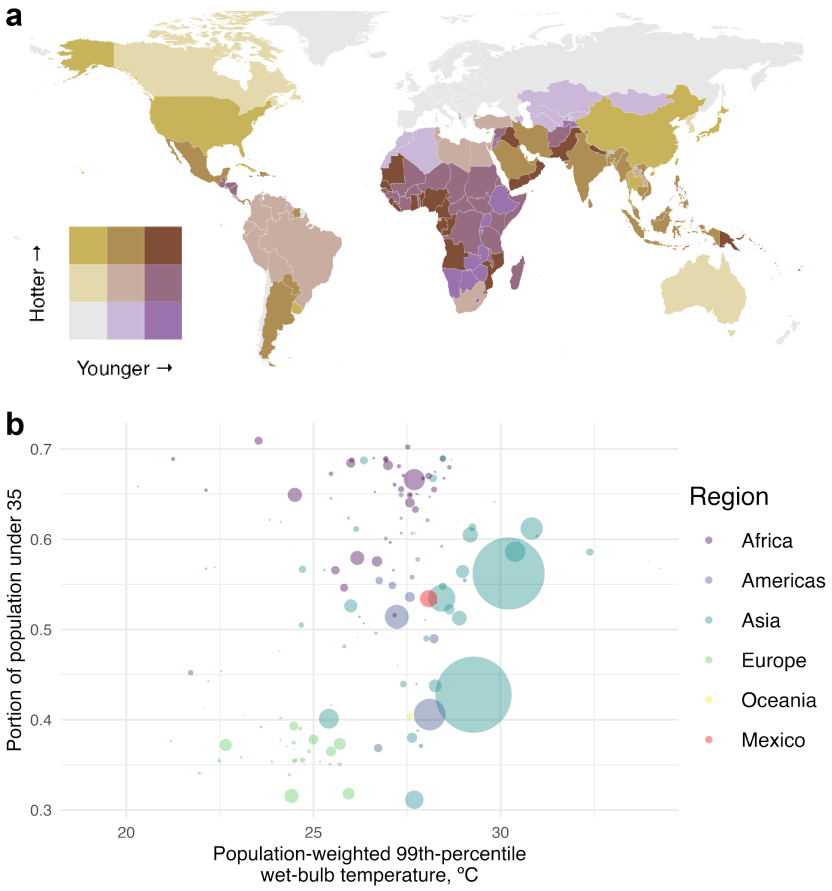


Figure S12: Historical extreme wet-bulb temperature exposures and current portion of population under 35
a. Countries colored according to their tercile of the global distribution of (1) historical extreme wet-bulb temperature exposures: 99^{th} percentile of population-weighted exposures, with temperatures estimates by [32] using ERA-5 Interim values from 1979 to 2017 and population distribution information from [80] and (2) portion of 2010 population under 35 [69]. **b.** Scatterplot of country-level historical extreme wet-bulb temperature exposure and the portion of the 2010 population under 35. Points are scaled according to total population size.

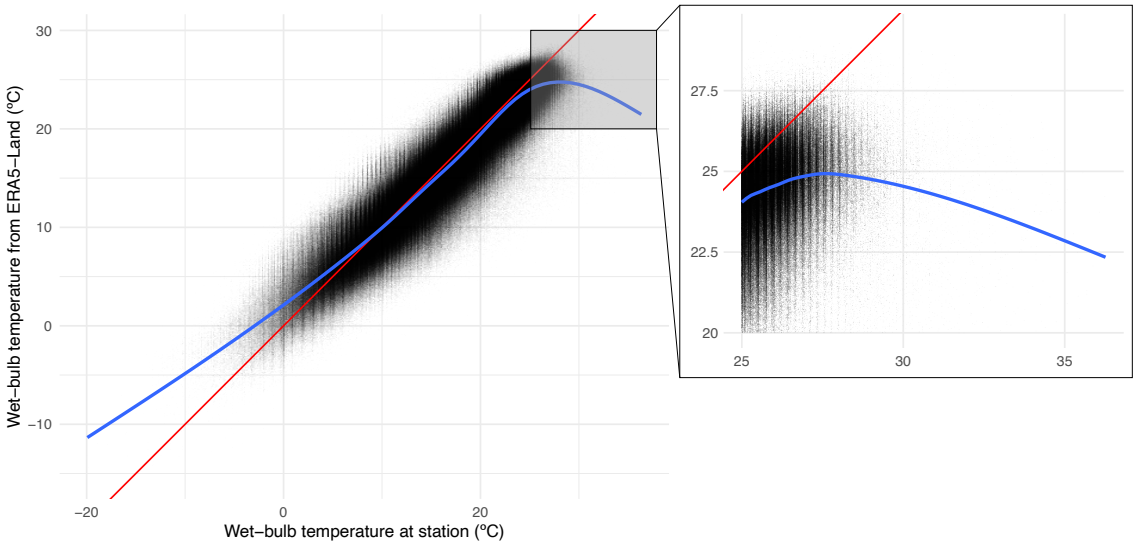


Figure S13: Daily average wet-bulb temperatures recorded at stations and in ERA5-Land

Data spans the period 1998–2019. Each point represents a pair of observations at a weather station (mean of sub-daily values) in Mexico and the corresponding value of ERA5-Land at that position and time (mean of hourly values). The blue line is a generalized additive model of cubic regression splines estimated by REML. The red line, for comparison, illustrates what would be observed with a one-to-one correspondence.

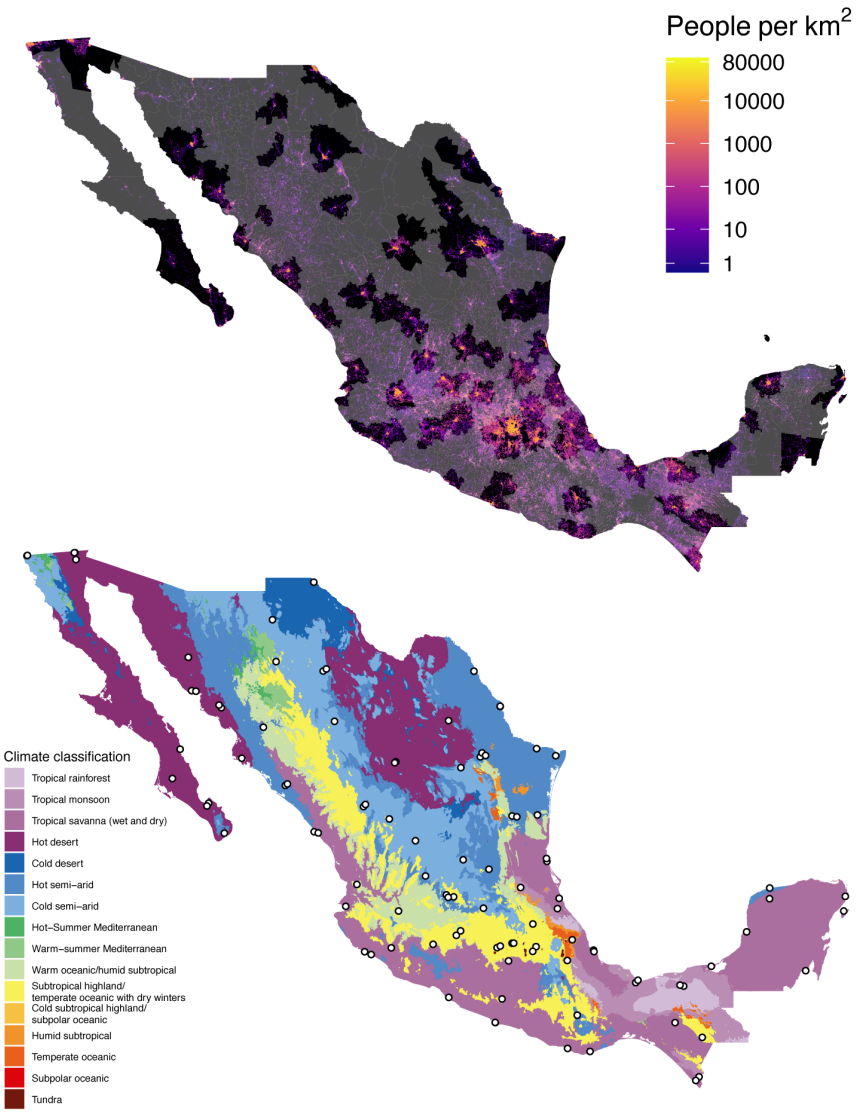


Figure S14: Map of population, municipalities, weather monitor locations, and climate zones in Mexico

The top panel of this figure shows the population density of Mexico (background color gradient) in the municipalities analyzed. The subset of municipalities dropped from our analysis (because they are too far from weather stations) are grayed out. The bottom panel of this figure shows the location of weather stations used in our analysis (white points with black outlines) and Köppen climate zones (background color gradient).